University of Alberta

BEHAVIOR OF SHALE CAPROCK UNDER EXPOSURE TO SUPERCRITICAL CO_2

by

Ming Liu

A thesis submitted to the Faculty of Graduate Studies and Research
in partial fulfillment of the requirements for the degree of

Master of Science
in
Geotechnical Engineering

Department of Civil and Environment Engineering

Fall 2013
Edmonton, Alberta

Abstract

A systematic set of experiments was carried out on Lea Park shale samples from the Pembina Cardium Field in west-central Alberta, Canada. Batch reaction tests were conducted on multiple, small shale specimens bonded to an acrylic polymer substrate to investigate geochemical alterations induced by exposing brine/CO_2 mixtures at designed pressure and temperature with both CO_2 and compressed air. Different surface monitoring technologies were applied at the same time. To understand the behavior of CO_2 plume, capillary entry pressure and permeability measurements were also carried out at in situ pressure and temperature conditions to evaluate the caprock integrity under the operation of CO_2 injection. The Lea Park shale caprock is a fissured clayey material, which was very reactive upon exposure to CO_2/brine. Rock/brine/CO_2 interactions leads to dissolution of illite, meanwhile, a cluster-coating structure with different geometries was observed on the rock surface in batch reaction tests. This coating disappears over time followed by the precipitation of new clay mineral dominated material on the surface of rock.

For caprock sealing efficiency, a very low CO_2 capillary entry pressure of 700 kPa was measured for this caprock material, which may indicate poor capillary sealing efficiency. However, the permeability of Lea Park shale is ultra-low (less than 1nD) so even though CO_2 may easily penetrate into the caprock formation due to its low capillary entry pressure, it will effectively be trapped due to its ultra-low permeability.

Acknowledgments

I could never overstate my great thanks to my supervisor, Dr. Rick Chalaturnyk, for his expertise, courage, motivation, patience, understanding and generous supports to my master study. He not only provided me with technical skills but also taught me the spirit that never gives up easily when facing difficulties. He became more of a guiding people and friend than a professor.

Great thanks must go to professors in geotechnical group (Dr. Dave Chan, Dr. Derek Martin, Dr. Dave Sego, and Dr. Wilson) for their wonderful help in enriching my knowledge in geotechnical engineering. Your rigorous academic attitude, detailed explanations and wise word in the class made my master study a precious experience in my life.

I would thank all the members in Reservoir Geomechanics Research Group (RG^2) for your endless help and encouragement in the laboratory, especially Steve Gamble, Gilbert Wong and Nathan Deisman.

I need to express my deepest feelings to my love family for their care, encouragement, support regardless of happiness or sadness; I could not make this journey without you.

At last, I want to thank Helmholtz-Alberta Initiative for funding this research program.

Table of Contents

List of Figures

List of Tables

1. Introduction

1.1 Statement of the Problem

Greenhouse gas effect is a rising problem well known for its contribution in increasing global temperature that may potentially result in severe environmental issues. Canada, in 2009, reported total greenhouse gas emissions (carbon dioxide equivalent) of 249.5 Mt (megatonnes), as shown in Figure 1-1, while for Alberta, the total was 113.1 Mt [1], comprising almost half of Canada's greenhouse emissions. CO_2 takes up 96.8% among all types of greenhouse gases (Figure 1-2) [1]. Therefore, it is of great importance for Alberta to reduce anthropogenic CO_2 emission significantly.

In Alberta's 2008 Climate Change Strategy, the Government of Alberta committed to reduce 20, 50 and 200 MT provincial emissions by the year 2010, 2020 and 2050, respectively. Among the three major reduction options, Carbon Capture and Storage (CCS) is expected to contribute almost 140MT of total emission reduction (Figure 1-3) and in the same year, the Government of Alberta committed $2 billion to fund CCS projects.

For the geological storage of CO_2, public safety and environmental issues related to the permanent sequestration of the CO_2 requires that competent barriers (caprocks or seals) are present above the CO_2 injection zone to prevent the injected CO_2 from escaping to the surface. Before implementing any CCS project, caprock integrity must be carefully examined. Low permeability formations such as shale or anhydrite, common formations encountered in Alberta sedimentary

basin, provide potential candidates for caprock material. The impact of shaly caprock/brine/CO_2 interactions and their impact on caprock integrity are studied in this research programme.

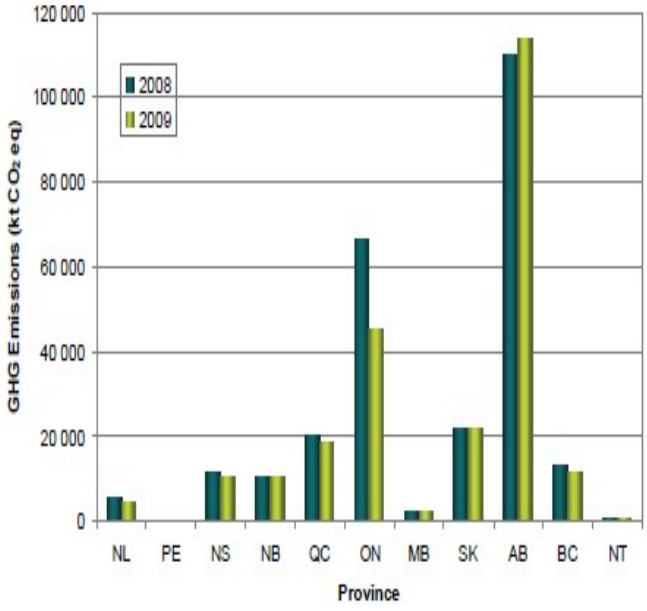

Figure 1-1 Greenhouse gas emission across Canada in 2009 (Environmental Canada, 2010)

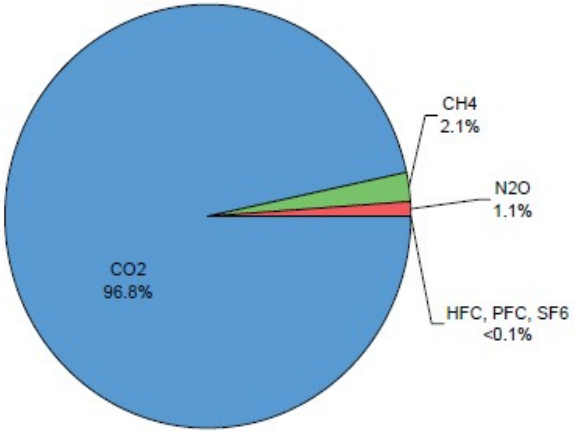

Figure 1-2 Alberta greenhouse gas emissions in 2009 (Alberta Environment, 2011)

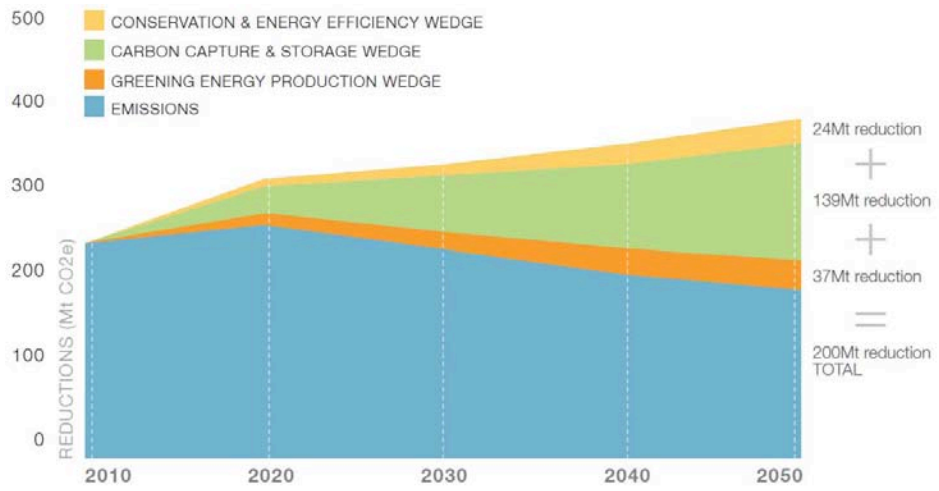

Figure 1-3 Greenhouse Gas Reduction Wedge (Alberta Environment, 2008)

1.1 Objectives and Scope

The objective of this research has a focus on caprock/brine/CO_2 interactions and their impact on assessment of shale formations as suitable caprocks for geological storage of CO_2. The main research objective is the execution of an experimental investigation on caprock/brine/CO_2 interactions. This research objective is subdivided into three categories:

- Surface chemical composition alternation introduced by caprock/brine/CO_2 interactions.
- Analyze the impact of caprock/brine/CO_2 interactions on caprock surface structures.
- Examination of caprock integrity (permeability and capillary pressure) under the condition of CO_2 injection.

1.2 Organization of Thesis

The basic concept of CO_2 geological storage is presented in Chapter 2 followed with a detailed summary of previous rock/brine/CO_2 interactions research in

Chapter 3. The source of the shale caprock, sampling method and previous investigations on this material are discussed in Chapter 4. Laboratory testing equipment, methods and experimental results are described in Chapters 5, 6 and Appendix A to D. Major conclusions and recommendations for further work are summarized in Chapter 7. Reference is attached at the last of each chapter.

1.3 Reference

1. Alberta Environment, 2011. Report on 2009 Greenhouse Gas Emissions. 27 p.

2. Alberta Environment, 2008. Alberta's 2008 Climate change strategy, Responsibility/Leadership/Action. 29 p.

3. IPCC, 2005: IPCC Special Report on Carbon Dioxide Capture and Storage. Prepared by Working Group III of the Intergovernmental Panel on Climate Change [Metz, B., O. Davidson, H. C. de Coninck, M. Loos, and L. A. Meyer (eds.)]. Cambridge University Press, Cambridge, United Kingdom and New York, NY, USA, 442 pp.

4. Gunter, W., S. Bachu, D. Law, V. Marwaha, D. Drysdale, D. Macdonald and T. Mccann, 1996. Technical and economic feasibility of CO_2 disposal in aquifers within the Alberta sedimentary basin, Canada. Energy Conversion and Management, Vol. 37, pp.1135-1142.

5. Bachu, S., 2000. Sequestration of CO_2 in geological media: criteria and approach for site selection in response to climate change. Energy Conversion and Management, Vol. 41, pp. 953-970.

6. Alberta Carbon Capture and Storage Development Council, 2009. Accelerating Carbon Capture and Storage Implementation in Alberta, Final Report. 71 p.

7. Environment Canada, 2010. Overview of the Reported 2009 Greenhouse Gas Emissions. 11 p.

2 Geological Storage of CO_2

Carbon Capture and Storage (CCS), also known as Carbon Capture and Sequestration, is the separation and capture of carbon dioxide (CO_2) from the atmospheric emissions of industrial processes and the transport and permanent storage of the CO_2 in deep underground rock formations. By preventing CO_2 from large-scale industrial facilities from entering the atmosphere, CCS is a powerful tool for combating climate change. Geologic storage is the component of CCS in which the CO_2 is disposed of underground. Geologic storage is also sometimes called "geologic sequestration" or "geosequestration".

2.1 Geological Storage Options

Carbon storage in geological formations is considered a promising method to mitigate the impact of greenhouse gas effect introduced by greenhouse gases such as CO_2, CH_4 etc. Depleted oil and gas reservoir, unmineable coal seam and deep saline aquifer are three major potential storage options. Table 1 shows their estimated storage capacity [1].

Table 2-1 Storage capacity of several geological storage options. (IPCC, 2005).

Reservoir type	Lower estimate storage capacity ($GtCO_2$)	Upper estimate of storage capacity ($GtCO_2$)
Deep saline formations	1,000	Uncertain, but possibly 10^4
Unminable coal seams (ECBM)	3-15	200
Oil and gas fields	675[a]	900[a]

[a] These numbers would increase by 25% if 'undiscovered' oil and gas fields were included in this assessment.

2.1.1 Deep Saline Formations

In almost all sedimentary basins around the world, deep saline formations possess the largest storage capacity for carbon geosequestration. They have a very promising upper estimated CO_2 storage capacity of approximate 1,000 to 10,000Gt and are widely spread around the world in contracts to hydrocarbon reservoirs that are more geographically restricted.

A successful example of carbon geosequestration in a saline formation is the Sleipner Project, North Sea. Supercritical carbon dioxide has been injected into Utsira sandstone reservoir at a rate of approximate 1Mt/year since 1996 and the total estimated carbon dioxide storage would be 20Mt by the end of this project [1] [2]. Until 2009, 2/3 of the injected CO_2 still had not reached the base of the shale caprock [3].

2.1.2 Coal Seams

CO_2 storage in coal seams, also known as carbon dioxide enhanced coal bed methane (CO_2 - ECBM), is an attractive option for carbon geosequestration.

- The structure of coal seams (fractures and matrix structure) is ideal for carbon storage in a similar fashion to the way coal seams store methane and other gases.
- For pure gas, CO_2 sorption is approximately double of methane sorption since carbon dioxide has a greater affinity to coal than methane and the ratio could reach as high as 10 [4]. As a result, injected CO_2 could displace the stored methane as well as re-pressurizing the reservoir, thereby potentially increasing methane production. If captured, the excess methane

production can be sold to offset the cost of carbon storage. For Alberta, the estimated CO_2 storage capacity through CO_2 - ECBM is 20GT [5].

An example of this category is Allison Unit CO_2 – ECBM Recovery Pilot Project in the United States. The project started in 1989, in more than 6 years, 181 million m^3 CO_2 was injected into the reservoir and 277,000t CO_2 was permanently sequestered [1].

2.1.3 Oil and Gas Fields

Oil and gas reservoirs have the potential for valuable storage sites for the following reasons:

- Similar to CO_2 – ECBM, the structure of oil and gas reservoirs is ideal for CO_2 storage. A typical reservoir consists of a producing formation and an overlaying impermeable sealing formation that could arrest CO_2 for a long time in the same way that the seal traps the hydrocarbons;
- CO_2 flooding in mature and partially depleted oil reservoirs has been used as enhanced oil recovery (EOR) method for several decades (CO_2 - EOR). CO_2 injection can increase the mobility of crude oil by decreasing its viscosity. Previous studies showed CO_2 enhanced oil recovery has a potential of 3.0-23.5% original in place oil [1] [8] [9]. Besides, enhanced oil production can offset part of the carbon storage cost and provide funding for related research. It is estimated that Alberta has a 3.5 billion barrels oil recovery potential if the oil price stays over $125/barrel while storing over 1100Mt CO_2 [9]; and
- Oil and gas reservoirs that are either under exploition or already depleted are technically well understood. Reservoir structures are fully investigated and reservoir monitoring as well as modelling technologies are more

developed. At the same time, use of existing infrastructures such as wells and pipelines has the potential to decrease the cost of carbon storage.

A successful case of CO_2 - EOR project is Cenovus's Weyburn Project in southeastern Saskatchewan, Canada. The project started in 2000 and had already injected 18MT CO_2 by 2010. As a result of this ten-year injection, oil production of Weyburn field has raised by 60% and the finally increment is estimated to be 155 million barrels and 60 million barrels for the adjacent Midale field [10].

2.1.4 Trapping Mechanisms

In order to guarantee CO_2 storage security, trapping mechanisms must be well understood. The four basic trapping mechanisms involved in carbon geosequestration are structural & stratigraphical trapping, residual trapping, solubility trapping and mineral trapping. Under certain conditions, adsorption trapping in coal bed and hydrodynamic trapping in extreme slow flow velocity reservoirs would be effective as well. These trapping phenomenons can be categorized into different types based on various classification methods.

- Physical and chemical trapping. Physical effect includes structural & stratigraphical trapping， adsorption trapping and residual trapping while chemical trapping consists of solubility trapping and mineral trapping. The time scale and security of fundamental trapping mechanisms are shown in Figure 2-1 [1].

- Preliminary and secondary trapping. After injection, CO_2 is initially stored by preliminary processes including structural & stratigraphical trapping and hydrodynamic trapping. Secondary trapping processes consist of residual trapping, solubility trapping and mineral trapping that take much longer time to evolve.

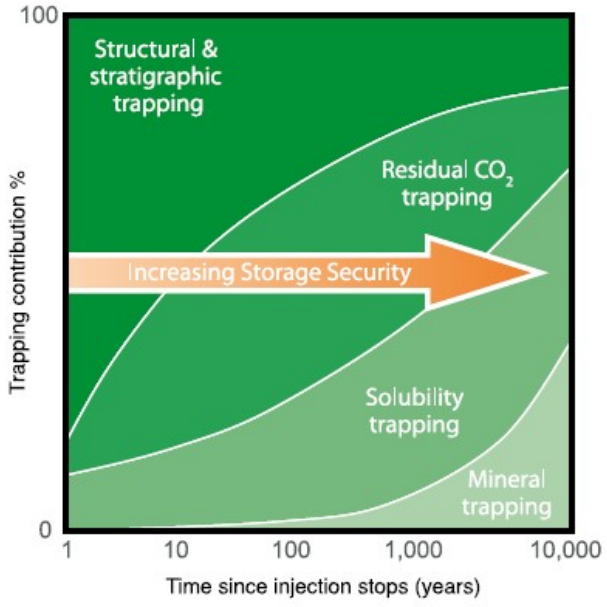

Figure 2-1 Storage security for different trapping mechanisms. (IPCC, 2005)

2.1.5 Structural and Stratigraphical Trapping

Carbon dioxide is usually injected in supercritical state, which is less dense than water, so the injected CO_2 plume will migrate upward due to buoyant force and be collected below the caprock. If a trapping structure is present geologically, then the CO_2 plume will accumulate within this structure. Stratigraphic trapping, which includes hydrodynamic trapping, occurs in a storage formation whose geometry doesn't have a trap and storage is governed by the lithology and slow hydrodynamic flow within those lithologies [1] [11].

2.1.6 Residual Trapping

Residual trapping, also known as irreducible gas saturation trapping, where CO_2 is trapped in pore space as immobile phase, is the result of interfacial tension. After injection, CO_2 (non-wetting phase) would displace formation brine (wetting phase) in the pore space, which is defined as drainage; when CO_2 injection

stopped, the return of the displaced wetting phase (formation brine) and the retreat of the non-wetting phase (CO_2) will result in incomplete displacement of the CO_2, trapping it in the pore space as an immobile phase. Figure 2-2 illustrates the residual trapping mechanism [12].

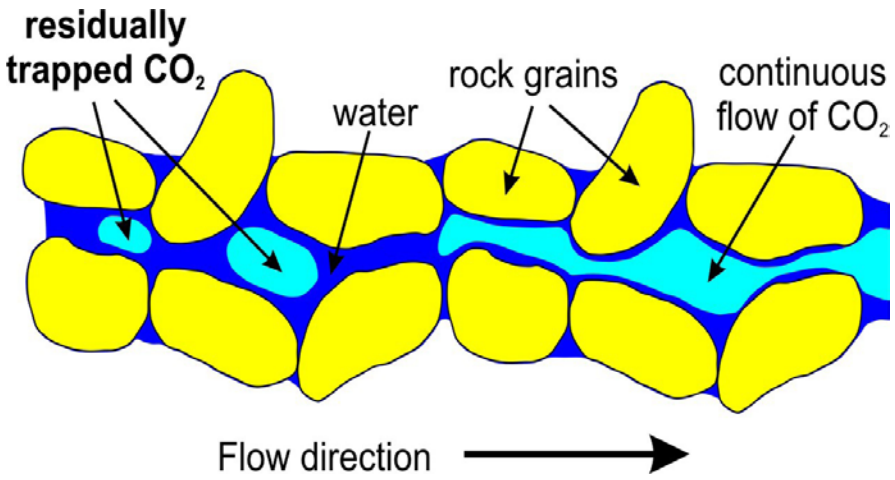

Figure 2-2 Residual trapping of CO_2 (CO2CRC, 2008)

2.1.7 Solubility Trapping

Once injected into the reservoir, CO_2 will dissolve into the formation water and the amount is a function of the pressure and temperature within the formation. The process could be described as:

$$CO_2 + H_2O \leftrightarrow H_2CO_3 \leftrightarrow H^+ + HCO_3^- \leftrightarrow 2H^+ + CO_3^{2-} + 2H^+$$

However, CO_2 dissolution into formation water is a slow process, thus solubility trapping is a time – dependant mechanism.

2.1.8 Mineral Trapping

Once CO_2 is dissolved in the brine, reactions with formation minerals such as calcium and magnesium will result in the precipitation of calcite and magnesium

carbonate. The creation of these minerals is called mineral trapping and is the most stable trapping mechanism since carbon dioxide is immobilized for a very long time scale. These geochemical reactions are very slow and occur over very long time scales, on the scale of hundreds to thousands of years. Since mineral trapping is quite variable from formation to formation, it should be examined during site characterization of each geological storage site [12].

2.1.9 Hydrodynamic Trapping

Hydrodynamic trapping can occur in saline formations that do not have a closed trap, but where fluids migrate very slowly over long distances, after reaching formation top, it would continue to migrate until trapped as residual gas saturation or in local structural or stratigraphic traps within the formation [1]. On a longer time scale, more and more CO_2 will be dissolved into formation water and move with formation water flow, for aquifers with extremely low flow velocity and long travel distance, CO_2 would stay in aquifers and move with formation water flow for millions of years before reaching surface, during that time, CO_2 should potential arrested by the combination of other trapping mechanisms. This process is called hydrodynamic trapping.

2.1.10 Adsorption Trapping

Adsorption trapping only occurs in coal seams and is the dominant storage mechanism in coal seams. The mechanism is due to coal has higher sorption capacity of CO_2 than methane and the volumetric trapping ratio between CO_2 and CH_4 is site dependant.

2.2 Chapter Summary

Deep saline formation, coal seam as well as oil and gas field are three major options for geological storage of CO_2. CO_2 will be arrested by both physical and chemical processes in different media with various trapping mechanisms occurring over different time-scales.

2.3 Reference

1. IPCC, 2005: IPCC Special Report on Carbon Dioxide Capture and Storage. Prepared by Working Group III of the Intergovernmental Panel on Climate Change [Metz, B., O. Davidson, H. C. de Coninck, M. Loos, and L. A. Meyer (eds.)]. Cambridge University Press, Cambridge, United Kingdom and New York, NY, USA, 442 pp.

2. Bickle, M., A. Chadwick, H. Huppert, M. Hallworth and S. Lyle, 2007. Modelling carbon dioxide accumulation at Sleipner: Implications for underground carbon storage. Earth and Planetary Science Letters, Vol. 255, pp. 164-176.

3. Hermanrud, C., T. Andresen, O. Eiken, H. Hansen, A. Janbu, J. Lippard, H. Bolås, T. Simmenes, G. Teige and S. Østmo, 2009. Storage of CO_2 in saline acquifers – lessons learned from 10 years of injection into the Utsira Formation in the Sleipner area. Energy Procedia, Vol. 1, pp. 1997-2004.

4. Shi, J. and S. Durucan, 2005. CO_2 Storage in Deep Unminable Coal Seams. Oil & Gas Science and Technology – Rev.IFP, Vol. 60, No. 3, pp. 547-558.

5. Gunter, W., T. Gentzis, B. Rottenfusser and R. Richardson, 1997. Deep coalbed methane in Alberta, Canada: A fuel source with the potential of zero greenhouse gas emissions. Energy Conversions and Management, Vol. 38, pp. S217-222.

6. Gunter, W., M. Mavor and J. Robinson, 2004. CO_2 Storage and enhanced coalbed methane production: field testing at Fenn-Big Valley, Alberta, Canada, with application. Proceedings of the 7th international conference on greenhouse gas control technologies, Vol. I, pp. 413-421.

7. Busch, A. and Y. Gensterblum, 2011. CBM and CO_2-ECBM related sorption process in coal: A review. International Journal of Coal Geology, Vol. 87, pp. 49-71.

8. Martin, F. and J. Taber, 1992. Carbon dioxide flooding. Journal of Petroleum Technology, Vol. 44, No. 4, pp. 396-400.

9. Alberta Carbon Capture and Storage Development Council, 2009. Accelerating Carbon Capture and Storage Implementation in Alberta, final report. 71 p.

10. Whittaker, S., B. Rostron, C. Hawkes, C. Gardner, D. Whit, J. Johnson, R. Chalaturnyk and D. Seeburger, 2011. A decade of CO_2 injection into depleting oil fields: monitoring and research activities of the IEA GHG Weyburn-Midale CO_2 Monitoring and Storage Project. Energy Procedia, Vol. 4, pp. 6069-6076.

11. Bachu, S., 2008. CO_2 storage in geological media: Role, means, status and barriers to deployment. Process in Energy and Combustion Science, Vol. 34, pp. 254-273.

12. CO2CRC, 2008. Storage Capacity Estimation, Site Selection and Characterisation for CO_2 Storage Projects. Cooperative Centre for Greenhouse Gas Technologies. Canberra. CO2CRC Report No.RPT08-1001. 52 p.

13. Bachu, S., Didier. Bonijoly, J. Bradshaw, R. Burruss, S. Holloway, N. Christensen and M. Mathiassen, 2007. CO_2 storage capacity estimation: Methodology and gaps. International Journal of Greenhouse Gas Control, Vol. I, pp. 430-443.

3 Caprock/Brine/CO_2 Interactions and Fluid Transportation Measurement

In this chapter, previous laboratory studies on rock/brine/CO_2 interactions are reviewed. Meanwhile, a review of permeability and capillary entry pressure measurement in low permeability rocks (shale) relevant to CO_2 storage is carried out.

3.1 Caprock Rock/Brine/CO_2 Interactions

In a storage complex or system, caprock is usually defined as a formation with very low permeability that is immediately overlying the CO_2 storage reservoir and ensures the injected CO_2 will stay (vertically, at least) within in storage formation. If CO_2 migrates through caprock, it could contaminant shallow drinking water aquifers and a quick release of large amounts of CO_2 can potentially be deadly, due to its asphyxiation properties or lead to significant environmental harm. So, as part of the site characterization studies of a geological storage site, long-term caprock performance after CO_2 injection must be carefully examined.

Once injected, CO_2 would begin to rise upward due to the buoyant force until it reaches the bottom of overlying caprock [4] [5]. At the same time, CO_2 will begin to dissolve into the formation brine after injected into target reservoir. When CO_2 dissolves into brine, it will release H^+ and lead to acidification of formation brine. This CO_2 charged brine will start to interact with contacted rock materials, both host rock and caprock, through processes generally referred to as rock/brine/CO_2 interactions. Due to these interactions, physical properties of rock

are potentially alterable and uncertainty in how these properties change due to long-term geochemical reactions is a critical issue when evaluating long time containment safety.

Most of previous studies on rock/brine/CO_2 interactions focus only on reservoir rocks especially carbonate and siliciclastic rocks, because it is related to oil recovery and mineral trapping capacity [6]-[10]. Figure 3-1 shows mineral changes in a siliciclastic aquifer after CO_2 injection. However, long-term caprock/brine/CO_2 interactions and their impact on sealing properties of the caprock still remain less studied [3]. Understanding these interactions on caprock sealing capacity is one of the critical factors in carbon storage since it relates directly to public and environment safety.

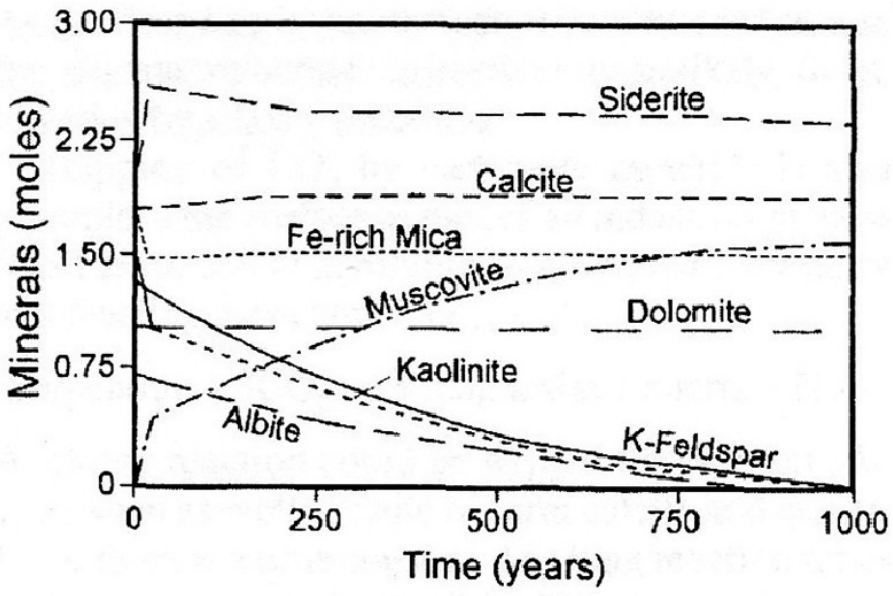

Figure 3-1 Water-rock reaction after CO_2 injection in a siliciclastic aquifer (from Gunter et al, 2000)

3.1.1 Experimental Research on Caprock/Brine/CO_2 Interactions

Limited laboratory experiments conducted on caprock materials have been reported in the literature [3], [11] to [18]. Similar to reservoir rock studies, a common test method for evaluating caprock/brine/CO_2 interactions is to place supercritical CO_2 or CO_2-saturated brine and caprock samples in batch reactors or triaxial cells, then increase the pressure and temperature to study the geochemical reactions, such as the one shown in Figure 3-2 [16].

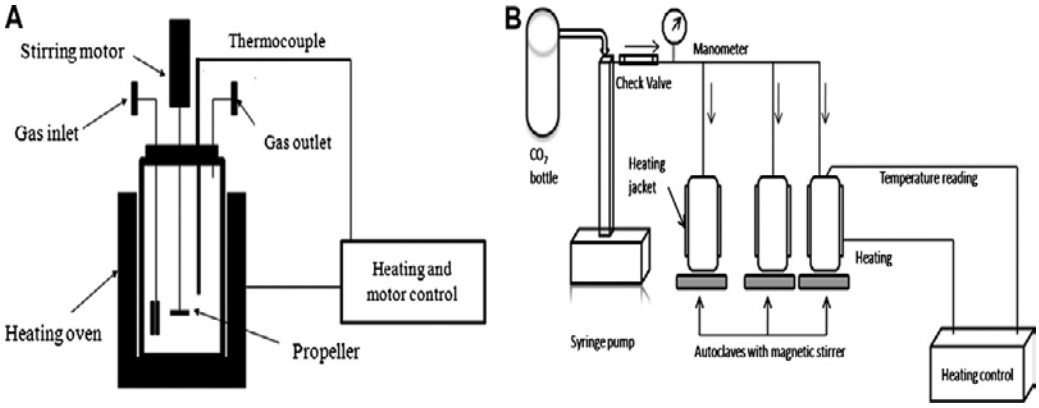

Figure 3-2 Experimental set-up for batch reaction test (from Alemu et al, 2011)

Batch reaction tests had been conducted on a modelled aquifer-aquitard system [11] [12]. Arkose and Silurian Maplewood shale samples from Monroe County, New York, USA were selected as aquifer and aquitard representative material, respectively with NaCl as pore fluid. Mineralogy analysis by X-ray diffraction indicates this shale has 65% clay minerals, 27% quartz, 5% K-feldspar and 2% of chlorite. CO_2 was injected into this fluid-rock system after 772 hours and the total reaction time was set at 1845 hours. Both brine chemistry and solid mineralogy were analyzed at the end of test. In addition, a pure rock-brine interaction was performed for comparison and all the tests were carried out at 200°C and 200 bars.

A decrease in pH from 4.9 to 4.1 was observed after CO_2 injection and then remained stable till the end of the test (Figure 3-3). Carbonate precipitations were observed in the rock-brine-CO_2 system compared with no precipitation in the pure rock-brine system, suggesting that shale contained reactive minerals. However, injection of CO_2 into the system increases the pressure in batch reactor from 200 to 254 bars with a total decrease of 24 bars over the following 39 hours. As a result, the pressure in rock-brine-CO_2 system is not consistent with the pressure in the rock-brine system. Clay mineralogy and their evolution were not covered in this study despite the fact that 65% of the shale is comprised of clay minerals [2].

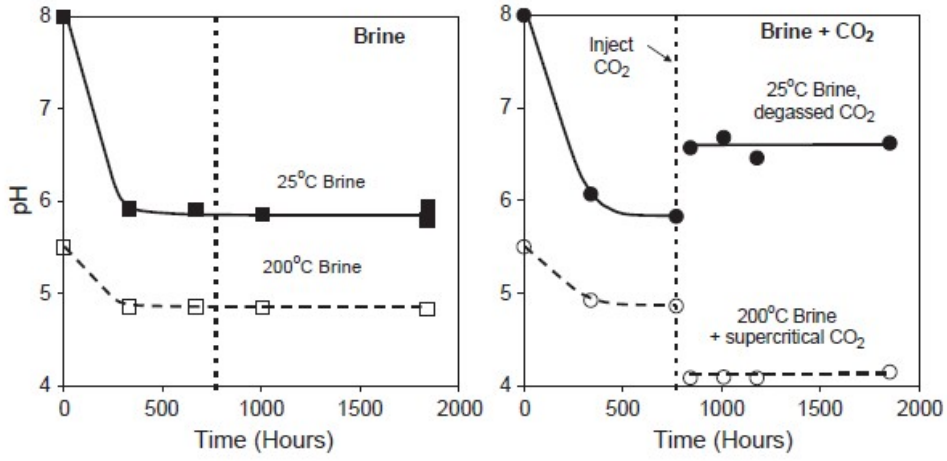

Figure 3-3 pH change in a rock-brine-CO_2 system (from Kaszuba et al, 2005)

Batch reaction tests on two caprock samples had been reported: one is clayey caprock from Chinle Formation, Utah, USA; the other is a clayey limestone from Comblanchien reservoir/caprock transition area in Charmotte, Paris Basin, France [13]. For mineralogy, Chinle shale comprised of 40% illite/smectite, 40% quartz, 10% calcite, 7% hematite and 3% calcite B (which is similar to dolomite), while the Comblanchien limestone was composed of 45% calcite, 15% illite/Smectite,

10% kaolinite, 10% quartz, 5% gypsum, 5% pyrite and 5% others. Experiments were carried out continuously up to 1 year under the temperature and pressure range from 80 to 150°C and 1 to 150 bars, respectively. The pH was observed to decrease after CO_2 injection, followed by partial or total dissolution of carbonate minerals. Also, complex carbonate mixture and partial dissolution of kaolinite were identified. Meanwhile, increase in Ca^{2+}, K^+ and Mg^{2+} indicates potential for secondary clay precipitation [2].

Batch reaction tests were also carried out on caprock samples from Callovo-Oxfordian Formation at St Martin de Bossenay, France [14]. X-ray diffraction showed that all the three caprock samples comprised mainly of quartz, calcite, dolomite and orthoclase. Both powdered and centimeter scale rock chips were exposed to fluid with different H_2O/CO_2 ratios at 150°C and 150 bars. Carbonate precipitation and secondary clay promotion were observed. However, the relatively high test temperature (150°C) and pressure (150 bars) compared to in situ reservoir condition at 70°C and 100 bars could accelerate reaction rates, but would also introduce potential inconsistency between laboratory experiments and field observations.

Batch reaction tests on Muderong Shale from Northwestern Shelf of Australia have been reported [15]. Crushed shale samples were exposed to CO_2 at 50°C and 15 MPa for up to 768 hours. X-ray diffraction tests were performed at different time intervals to evaluate mineralogy alteration with time (Figure 3-4). It was found that clay mineral alternation was the dominate mechanism in Muderong

Shale. One of their key contributions, besides the batch reaction test was an excess CO_2 sorption test on the same shale material. They found that it could physically adsorb significant amount of CO_2, a mechanism which usually is not included in primary storage capacity estimation.

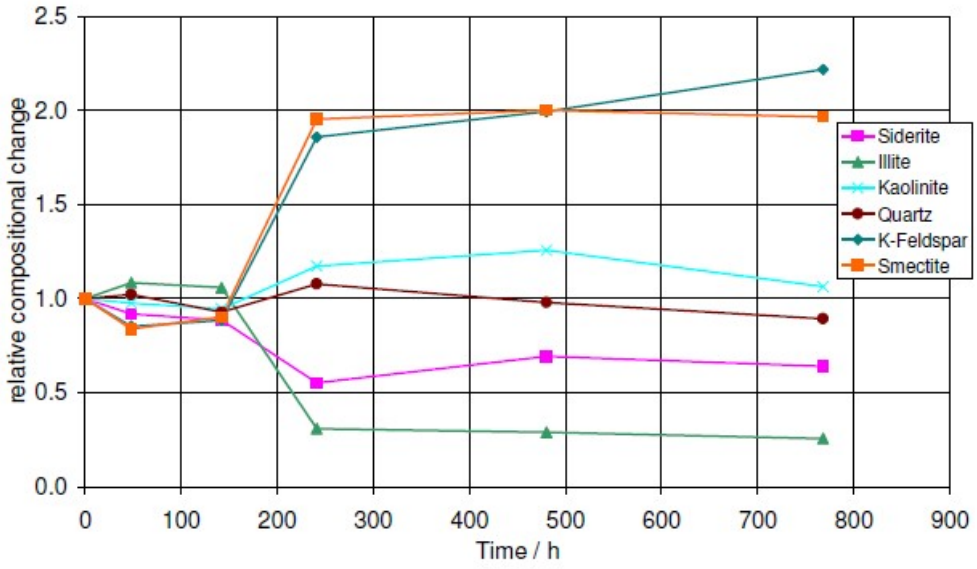

Figure 3-4 Mineralogy alteration in Muderong Shale (from Busch et al, 2009)

Batch reaction tests were also performed on crushed caprock samples from Adventdalen Group and Janusfjellet Subgroup, Svalbard, Norway [16]. Both samples (one is carbonate-rich shale while the other one is clay-rich shale) were exposed to CO_2-rich brine (NaCl) at temperature and pressure range from 80 to 250°C and 110 bars for a period of up to 5 weeks. In addition, an extra blank test using CO_2-free brine as a reference was also carried out, but with a decreased pressure at 40 bars. Both fluid and solid phase were analyzed at the end of test. Major discoveries include significant dissolution and followed by re-precipitation of carbonate, K-feldspar dissolution, clay mineral alternation and secondary

promotion of clay minerals. Also, they showed that carbonate-rich shale is more reactive than clay-rich shale. However, different pressure condition between rock-brine-CO_2 and rock-brine interactions brings uncertainty to the generality of this observation.

Batch reaction test on Eau Claire Formation Shale comprised mainly of quartz, orthoclase, illite and chlorite were also reported [2]. Shale sample was first placed in reactor with brine at 200°C and 300 bars for 23 days, then, CO_2 was introduced into the system to trigger rock-brine-CO_2 interactions, after another 23 days, temperature was reduced to 56°C and remain unchanged for a week to correspond to reservoir condition. Major geochemical observations included minor corrosion of feldspar and precipitation of secondary minerals.

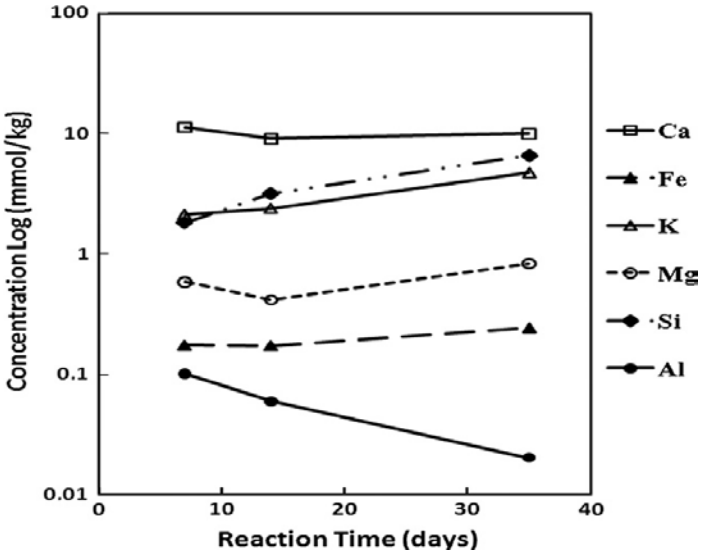

Figure 3-5 Brine chemistry as a function of reaction time (from Alemu et al, 2011)

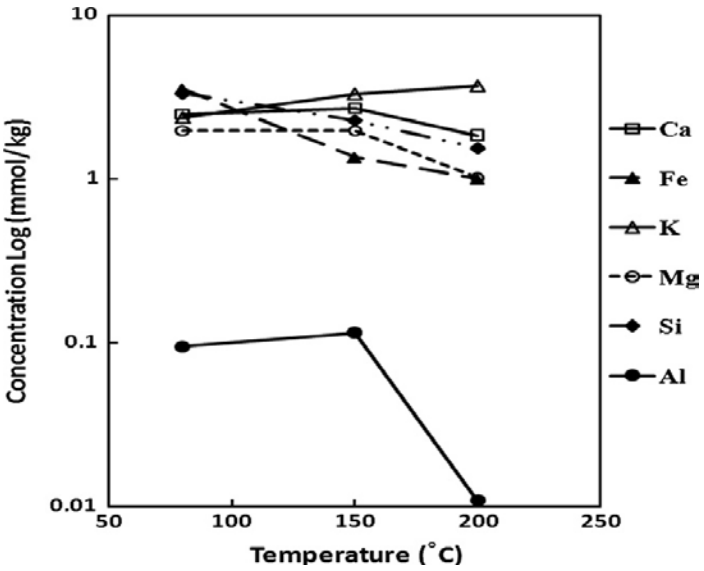

Figure 3-6 Brine chemistry as a function of temperature (from Alemu et al, 2011)

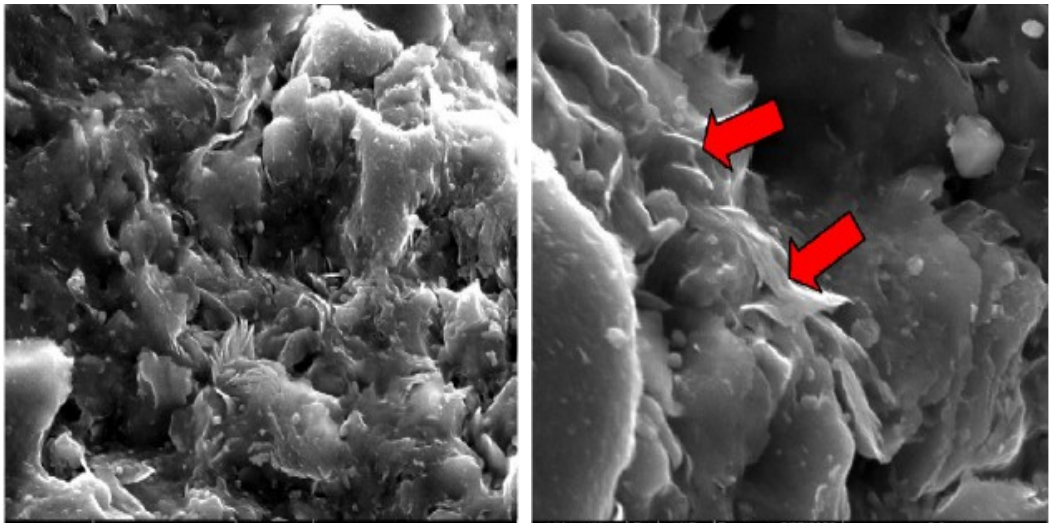

Figure 3-7 Secondary clay mineral precipitation for EAU shale (from Liu et al, 2012)

It is noticed from previous caprock/brine/CO_2 interaction reports that caprocks are generally reactive material when exposed to CO_2/brine mixtures and some common features were observed:

- Acidification of brine;
- Dissolution and re-precipitation of carbonate;
- Minor corrosion of K-feldspar;
- Alternation of clay minerals;
- Secondary clay mineral precipitation; and
- CO_2 sorption capacity that would enhance the storage capacity.

3.2 Fluid Transportation Measurement

3.2.1 Permeability Measurement (Brace's Pulse-Decay Method)

As mentioned before, after injection, CO_2 would rise upward due to buoyancy until stopped by caprock. However, if the accumulated CO_2 column is too high, the generated pressure exceeded a threshold value (capillary entry pressure); CO_2 will penetrate and migrate through caprock. As well, dissolved CO_2 will flow through caprock with the pore fluid. As a result, one of the criteria when selecting caprock formation is to have ultra-low permeability.

In a porous media, permeability is a measure of rate of fluid flow under a pressure gradient and it is widely accepted that Darcy's law best describes fluid flow through porous media:

$$Q = -\frac{kA}{\mu}\frac{\Delta P}{L} \qquad [1]$$

where: Q is the total volume of fluid per unit time through a cross-section [m^3/s];

k is the permeability[m^2];

A is the area of cross-section[m^2];

μ is the fluid viscosity[Pa·s];

ΔP is the pressure drop between start and end point of flow path[Pa]; and

L is the length of flow path[m].

Standard permeability measurement methods used in the laboratory are based on flow rate and hydraulic gradient measurements after steady-state flow is established through the specimen. However, in low permeability materials such as shale, this is difficult and impractical.

In order to measure permeability of Westerly Granite, which is a rock with ultra-low permeability, a method that is known as the pulse-decay method was developed [21]. Ever since, the method has become popular due to shorter testing time and accurate measurement results. The basic concept of the pulse-decay method is to assume validation of Darcy's Law, then, apply a sudden pressure increase in upstream reservoir and then measure the pressure decay with time; permeability is calculated based on the pressure-time relationship.

The experiment setup is shown in Figure 3-8. The testing specimen is sandwiched between two "reservoirs"; the upstream (R_1) consists of the center hole in the piston plus the volumes enclosed by tubing, valves and pressure transducer. The downstream (R_2) reservoir is the volume in the steel plug. Volumes of both reservoirs are defined as V_1 and V_2, respectively while pressures in two reservoirs are defined as P_1 and P_2. A confining pressure P_c is applied to the system and should be always kept greater than P_1 and P_2.

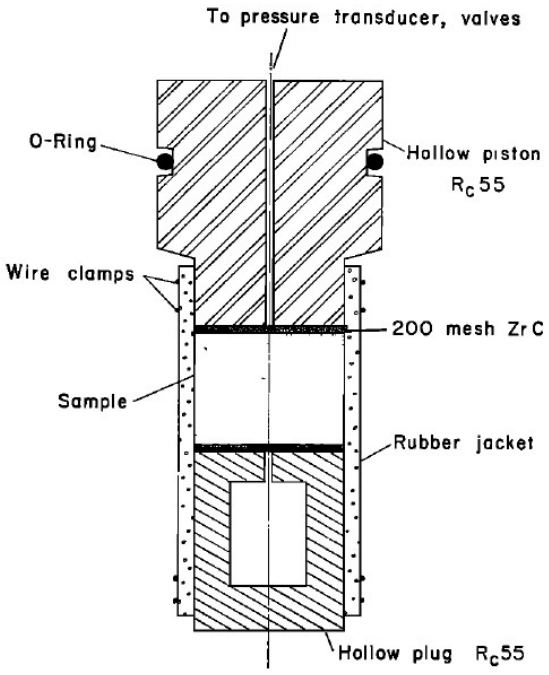

Figure 3-8 Experimental arrangement for pulse-decay method (from Brace et al, 1968)

At the beginning of the test ($t = t_0$), pressures in both reservoirs are equal and less than confining pressure ($P_1 = P_2 < P_c$), then, at t_0, pressure in upstream is increased by a small amount of ΔP (less than 10% of P_1). Then, pressure (P_1) in the upstream reservoir (R_1) will begin to decrease while pressure in downstream (P_2) reservoir will start to increase until a final equalization pressure of P_f is reached in both reservoirs. A typical pressure-time relationship is shown in Figure 3-9.

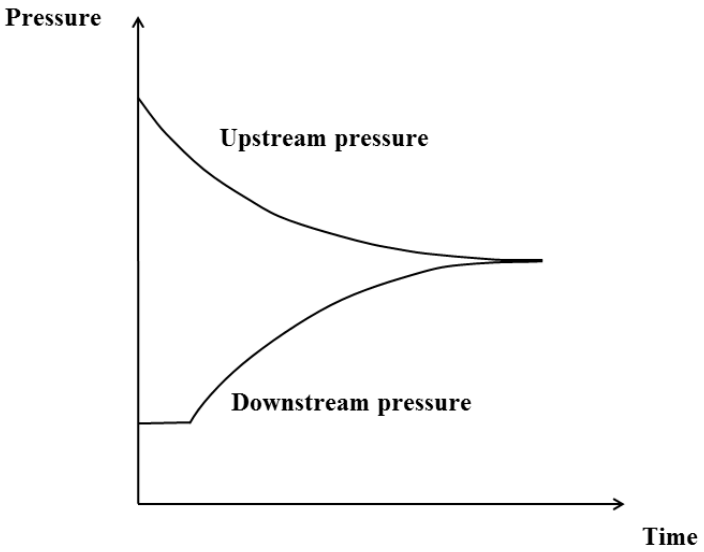

Figure 3-9 Typical pressure response in pulse-decay permeability measurement

Based on a semi-log plot of pressure decay versus time (Figure 3-10), permeability can be determined from the slope and the following equation:

$$\text{Slope} = -\frac{kA}{\mu\beta L}\left(\frac{1}{V1}+\frac{1}{V2}\right) \quad [2]$$

where: k is permeability [m^2];

A is the area of cross-section[m^2];

μ is the fluid viscosity[dyne·sec·cm^{-2}];

β is the fluid compressibility[cm^2·$dyne^{-1}$];

L is the length of sample[m];

V_1 is the volume of upstream reservoir[m^3]; and

V_2 is the volume of downstream reservoir[m^3].

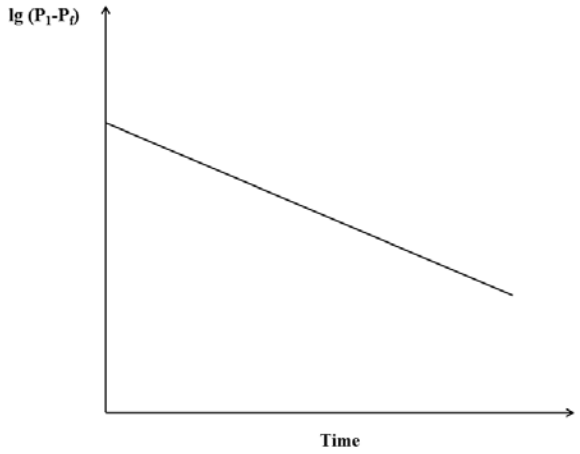

Figure 3-10 Typical pulse-decay permeability test result

Although conceptually simple, pulse-decay methods still present challenges experimentally. In Brace's test, it was assumed that sample porosity and compressive storage is very small and could be neglected. This assumption is reasonable in crystalline material such as Westerly granite; however, for material with significant porosity and compressive storage, this is a weak assumption [22]. In a later study, Trimmer found out that only the ratio of effective sample pore volume to the reservoir volume could introduce error to the permeability measurement using pulse-decay method and he suggested that in order to have a systematic error of l0% or less, the above ratio should be kept below 0.25[27]. Also, Lin points out that using $\log_{10}(P_1-P_f)$ instead of $\ln(P_1-P_f)$ will lower the value of permeability by a factor of 2.3[36].

3.2.2 Capillary Breakthrough Pressure Measurement

As mentioned before, once the CO_2 plume rises to the base of the caprock, the properties of the caprock need to sufficient to arrest the vertical movement of the

CO_2 and allow it to accumulate. As the CO_2 column accumulates, the buoyancy pressure is increasing and if it reaches a threshold value, CO_2 could penetrate and flow through the caprock. This critical pressure is usually referred to as the capillary breakthrough pressure.

The threshold pressure for a single fluid (non-wetting phase) entering a porous media saturated with another fluid (wetting phase) is described as:

$$Pc = \frac{2\gamma\cos\theta}{r} \quad [3]$$

where: Pc is the threshold pressure for the non-wetting phase to enter the media[Pa];

γ is the interfacial tension between two fluids[Pa·s];

θ is the contact angle[°]; and

r is the radius of the largest pore throat[m].

For supercritical state CO_2 injection into a brine-saturated formation, the formation brine is defined as the wetting phase and supercritical state CO_2 would be considered as the non-wetting phase. If the pressure difference between CO_2 and formation brine is large enough and exceeds the threshold pressure, CO_2 will penetrate into the caprock formation and cause caprock capillary integrity failure.

In order to maintain caprock integrity, measurement of threshold pressure or capillary breakthrough pressure is essential. The basic concept in measuring this critical value is to apply a non-wetting phase pressure at one end of a wetting phase saturated medium and then increase the pressure until the non-wetting phase reaches the other end of the sample [33] [34] [35]. The test method is

subdivided into two categories based on how pressure is increased: small pressure increment method and large pressure increment method.

Capillary entry pressure measurement using the small pressure increment method is described by Li et al [33]. A rock sample is placed between two porous stones and first saturated with the wetting phase. The non-wetting phase is then introduced into the inlet end at a low pressure level. A capillary tube is connected at the outlet of the sample to monitor the displaced liquid and once the movement of liquid meniscus in the tube is stable, a small injection pressure increment is applied. The suggested pressure increments were approximately 0.5-1.0MPa [33]. The above operations are repeated until a continuous slow liquid flow followed by a mixed flow with gas bubbles is observed. The pressure at the last step is considered as breakthrough pressure. A typical pressure result is illustrated in Figure 3-11.

Capillary breakthrough pressure measurement using the large pressure increment method was described by Hildenbrand et al. [34]. Similar to the small pressure increment method, a sample is sandwiched between two porous stones and saturated with a wetting phase fluid (usually formation brine). A high pressure gradient is instantaneously applied at the upstream side of the specimen and pressure changes in both reservoirs are recorded. The difference between finalized upstream and bottom stream pressure is defined as capillary pressure of the sample. Figure 3-12 shows a typical result of capillary pressure measurement with large increment method.

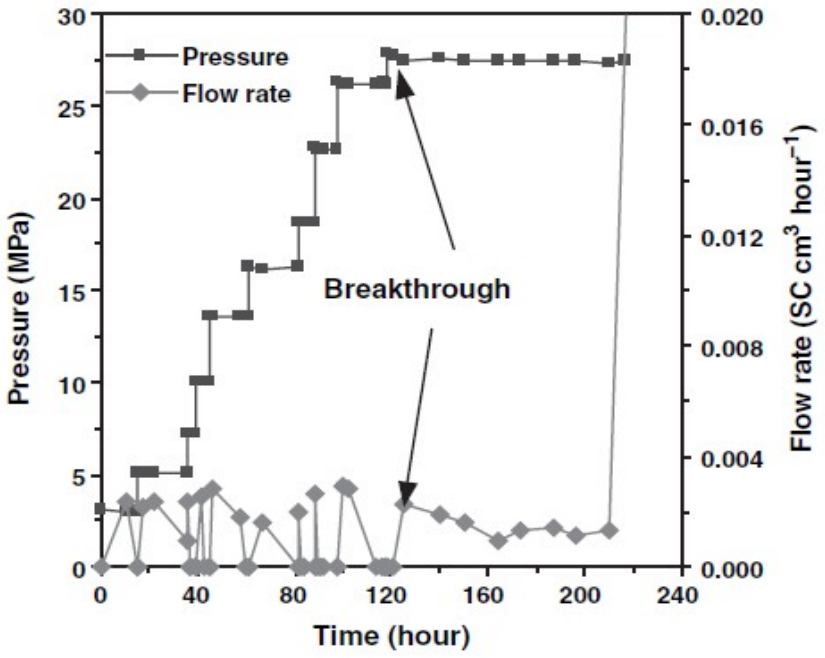

Figure 3-11 Experiment result for capillary pressure measurement using small increment method (from Li et al, 2005)

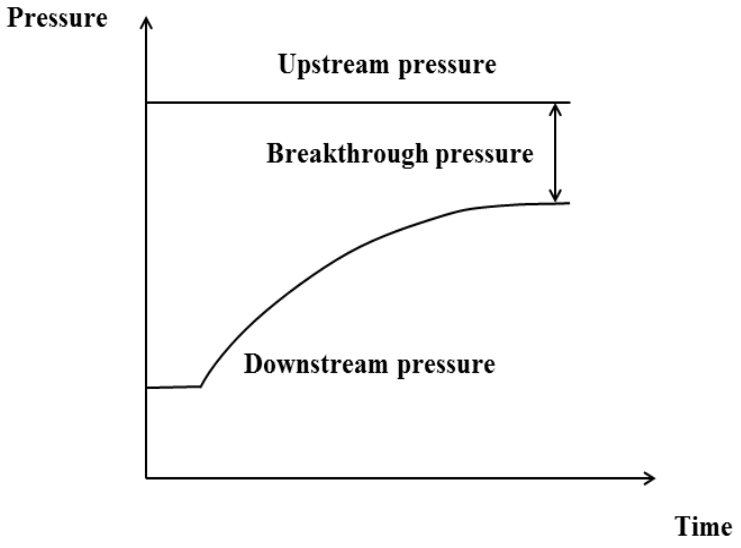

Figure 3-12 Experiment result for capillary pressure measurement using large increment method

Although conceptually similar, most of the previous investigations on capillary breakthrough pressure use gases as the non-wetting phase to penetrate brine saturated samples. However, in most of the deep underground storage cases, the formations that hold the injected CO_2 are deep enough that the in situ pressure and temperature are high enough to keep CO_2 in supercritical state, so in this research programme, supercritical state CO_2 is chosen as the non-wetting phase.

3.3 Chapter Summary

Reservoir rocks are popular materials in previous studies and very limited tests have been conducted on caprock materials. After injection, CO_2 will dissolve into formation brine and reduce its pH, causing dissolution and re-precipitation of carbonate and minor erosion of K-feldspar. Alternation and secondary precipitation of clay minerals are also popular features discovered. On the other hand, due to the nature of low-permeability, traditional steady-state permeability measurement is impractical and Brace's pulse-decay method should be adopted to generate more reliable test results.

3.4 Reference

1. Gaus, I., 2010. Role and impact of CO_2-rock interactions during CO_2 storage in sedimentary rocks. International Journal of Greenhouse Gas Control, Vol. 4, pp. 73-89.

2. Liu, F., P. Lu, C. Griffith, S. Hedges, Y. Soong, H. Hellevang and Z. Chen, 2012. CO_2-brine-caprock interaction: Reactivity experiments on Eau Claire Shale and a review of relevant literature. International Journal of Greenhouse Gas Control, Vol. 7, pp. 153-167.

3. Rochelle, C., Czernichowski-Lauriol. I and A. Milodowski, 2004. The impact of chemical reactions in CO_2 storage in geologic formations: a brief review. Baines, S.J, Worden, R.H.(Eds.), Geological Storage of Carbon Dioxide, Geological Society, London, Special Publication 233, pp.87-106..

4. Lindeberg, E. and P. Bergmo, 2003. The long-term fate of CO_2 injected into an aquifer. In: Gale, J., Kaya, Y.(Eds.), Proceeding of the 6th International Greenhouse Gas Control Technologies, Vol. I, pp. 489-494.

5. Baines, S. and R. Worden, 2004. The long-term fate of CO_2 in the subsurface: natural analogues for CO_2 storage. In: Baines, S.J, Worden, R.H.(Eds.), Geological Storage of Carbon Dioxide Special Publication of the Geological Society, Vol. 233, pp. 59-85.

6. Gunter, W., B. Wiwchar and E. Perkins, 1997. Aquifer disposal of CO_2-rich greenhouse gases: extension of the time scale of experiment for CO_2-sequestering reactions by geochemical modelling. Mineralogy and Petrology, Vol. 59, pp. 121-140.

7. Gunter, W., E. Perkins and I. Hutcheon, 2000. Aquifer disposal acid gases: modelling of water-rock reactions for trapping of acid wastes. Applied Geochemistry, Vol. 15, pp. 1085-1095.

8. Bowker, K. and P. Shuler, 1991. Carbon dioxide injection and resultant alteration of the Weber sandstone, Rangely Field, Colorado. American Association of Petroleum Geologists Bulletin, Vol. 75, pp. 1489-1499.

9. Grigg, R., B. McPherson and R. Svec, 2003. Laboratory and model tests at reservoir conditions for CO_2-brine-carbonate rock systems interactions. Proceedings of the Second Annual Carbon Sequestration Conference, Wastington, D.C., 17p.

10. Wellman, T., R. Grigg, B. McPherson, R. Svec and P. Lichtner, 2003. Evaluation of CO_2-Brine-Reservoir Rock Interactions with Laboratory Flow

Tests and Reactive Transportation Modeling. SPE Oilfield Chemistry Symposium, Paper SPE 80228, Houston, 9p.

11. Kaszuba, J., D. Janecky and M. Snow, 2003. Carbon dioxide reaction processes in a model brine aquifer at 200°C and 200 bar: implication for geologic sequestration of carbon. Applied Geochemistry, Vol. 18, pp. 1065-1080.

12. Kaszuba, J., D. Janecky and M. Snow, 2005. Experimental evaluation of mixed fluid reactions between supercritical carbon dioxide and NaCl brine: Relevance to the integrity of a geologic carbon repository. Chemical Geology, Vol. 217, pp. 277-293.

13. Credoz, A., O. Bildstein, M. Jullien, J. Raynal, J. Pétronin, M. Lillo, C. Pozo and G. Geniaut, 2009. Experimental and modeling study of geochemical reactivity between clayey caprocks and CO_2 in geological storage conditions. Energy Procedia, Vol. 1, pp. 3445-3452.

14. Kohler, E., T. Parra and O. Vidal, 2009. CLAYEY CAP-ROCK BEHAVIOR IN H_2O-CO_2 MEDIA AT LOW PRESSURE AND TEMPERATURE CONDITIONS: AN EXPERIMENTAL APPROACH. Clay and Clay Minerals, Vol 57, No.5, pp. 616-637.

15. Busch, A., S. Alles, B. Krooss, H. Stanjek, D. Dewhurst, 2009. Effect of physical sorption and chemical reactions of CO_2 in shaly caprocks. Energy Procedia, Vol. 1, pp. 3229-3235.

16. Alemu, B., P. Aagaard, I. Munz and E. Skurtveit, 2011. Caprock interaction with CO_2: A laboratory study of reactivity of shale with supercritical CO_2 and brine. Applied Geochemistry, Vol. 26, pp. 1975-1989.

17. Busch, A., S. Alles, Y. Gensterblum, D. Prinz, D. Dewhurst, M. Raven, H. Stanjek and B. Krooss, 2008. Carbon dioxide storage potential of shales. International Journal of Greenhouse Gas Control, Vol. 2, pp. 297-308.

18. Wollenweber, J., S. Alles, A. Kronimus, A. Busch, H. Stanjek and B. Krooss, 2009. Caprock and overburden processes in geological CO_2 storage: An experimental study on sealing efficiency and mineral alternations. Energy Procedia, Vol. 1, pp. 3469-3476.

19. Wollenweber, J., S. Alles, A. Busch, B. Kross, H. Stanjek and R. Littke, 2010. Experimental investigation of the CO_2 sealing efficiency of caprocks. International Journal of Greenhouse Gas Control, Vol. 4, pp. 231-241.

20. Gaus, I., M. Azaroual and I. Czernichowski-Lauriol, 2005. Reactive transport modelling of the impact of CO_2 injection on the clayey cap rock at Sleipner (North Sea). Chemical Geology, Vol. 217, pp. 319-337.

21. Brace, W., J. Walsh and W. Frangos, 1968. Permeability of granite under high pressure. Journal of Geophysical Research, Vol. 73, pp. 2225-2236.

22. Hsieh, P., J. Tracy, C. Neuzil, J. Bredehoeft and S. Silliman, 1981. A Transient Laboratory Method for Determining the Hydraulic Properties of 'Tight' Rocks—I. Theory. Int. J. Rock Mech. Min. Sci. & Geomech. Abstr, Vol. 18, pp. 245-252.

23. Neuzil, C., C. Cooley, S. Silliman, J. Bredehoeft and P. Hsieh, 1981. A Transient Laboratory Method for Determining the Hydraulic Properties of 'Tight' Rocks—II. Application. Int. J. Rock Mech. Min. Sci. & Geomech. Abstr, Vol. 18, pp. 253-258.

24. Metwally, Y. and C. Sondergeld, 2011. Measuring low permeabilities of gas-sands and shales using a pressure transmission technique. International Journal of Rock Mechanics & Mining Sciences, Vol. 48, pp. 1135-1144.

25. Jones, S., 1997. A technique for faster pulse-decay permeability measurements in tight rocks. SPE Formation Evaluation, Vol. 12, No. 1, pp. 19-25.

26. Wang, H. and D. Hart, 1993. Experimental Error for Permeability and Specific Storage from Pulse Decay Measurements. International Journal of Rock Mechanics and Mining Sciences & Geomechanics Abstracts, Vol. 30, No. 7, pp. 1173-1176.

27. Trimmer, D., 1981. Design criteria for laboratory measurements of low permeability rocks. Geophysical Research Letters, Vol. 8, No. 9, pp. 973-975.

28. Dicker, A. and R. Smits, 1988. A practical approach for determining permeability from laboratory pressure-pulse decay measurements. Presented at the SPE International Meeting in Petroleum Engineering, SPE Paper 17578, Tianjian, China, pp. 285-292.

29. Zhang, M., M. Takahashi, R. Morin and T. Esaki, Evaluation and Application of the Transient-Pulse Technique for Determining the Hydraulic Properties of Low-Permeability Rocks—Part 1: Theoretical Evaluation, Geotechnical Testing Journal, Vol. 23, No. 1, pp. 83-90.

30. Zhang, M., M. Takahashi, R. Morin and T. Esaki, 2000. Evaluation and Application of the Transient-Pulse Technique for Determining the Hydraulic Properties of Low-Permeability Rocks—Part 2: Experimental Application. Geotechnical Testing Journal, Vol. 23, No. 1, pp. 91-99.

31. Newsham, K., J. Rushing, P. Lasswell, J. Cox and T. Blasingame, 2004. A comparative Study of Laboratory Techniques for Measuring Capillary Pressures in Tight Gas Sands. SPE Annual Technical Conference and Exhibition, SPE 89866, Houston, Texas, USA, 11p.

32. Chiquet, P. and D. Broseta, 2005. Capillary Alternation of Shaly Caprocks by Carbon Dioxide. SPE Europec/EAGE Annual Conference, SPE 94183, Madrid, Spain, 10p.

33. Li, S., M. Dong, Z. Li, S. Huang, H. Qing and E. Nickel, 2005. Gas breakthrough pressure for hydrocarbon reservoir seal rocks: implications for

the security of long-term CO_2 storage in the Weyburn field. Geofluids, Vol. 5, pp. 326-334.

34. Hildenbrand, A., S. Schlomer and B. Kross, 2002. Gas breakthrough experiments on fine-grained sedimentary rocks. Geofluids, Vol. 2, pp. 3-23.

35. Hildenbrand, A., S. Schlomer, B. Kross and R. Little, 2004. Gas breakthrough experiments on pelitic rocks: comparative study with N_2, CO_2, and CH_4. Geofluids, Vol. 4, pp. 61-80.

36. Lin, W., 1981. Parametric analysis of the transient method of measuring permeability. Journal of Geophysical Research: Solid Earth, Vol 87, No. 2, pp. 1055-1060.

4 Pembina Cardium Project and Lea Park Shale

In order to encourage energy companies to use CO_2 for enhanced oil recovery and reduce annual CO_2 emission, the Government of Alberta instituted a $ 15 million royalty credit program in 2006. Four companies were selected for their pilot operations:

- Apache at Zama in northwestern Alberta
- Devon Energy at Swan Hills in central Alberta
- Penn West at the Pembina Cardium Field in west-central Alberta
- Anadarko at Enchants in southeastern Alberta

Ultimately, Pembina Cardium oil field was selected as the most suitable site for a pilot CO_2 monitoring project. Locations of above projects, especially the Pembina oil field were shows in Figure 4-1 [1].

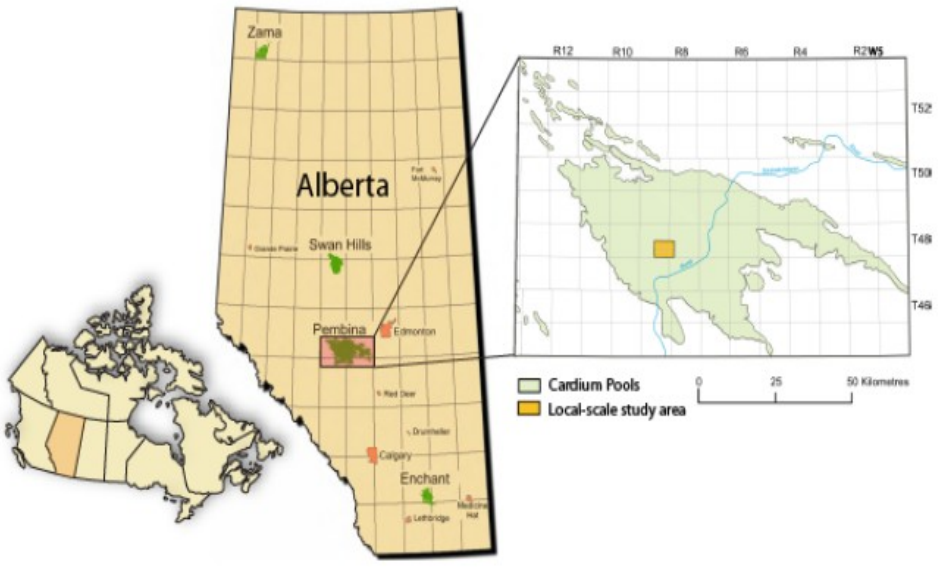

Figure 4-1 Location of the Enchant, Pembina, Swan Hill and Zama oil fields (from Lakeman et al, 2009)

4.1 Pembina Cardium Oil Field

4.1.1 Stratigraphy

Figure 4-2 shows the regional stratigraphy at the Pembina Field [2]. The Cardium Formation can be subdivided into four reservoirs: conglomerate, upper sandstone, middle sandstone and lower sandstone, respectively from top to bottom. The four reservoir units that form the Cardium Formation have a maximum cumulative thickness of about 20 meters and occur at depths ranging from 1600 meters in the northeast to 1650m in the southwest of the pilot site [3]. By far, the upper sandstone is the most productive reservoir and CO_2 was injected into this unit to enhance the oil recovery as well as carbon storage. The temperature in the Cardium Sandstone Formation is 50°C and initial pressure within the reservoir was approximately 19MPa [1]-[5].

4.1.2 Hydrogeology – Colorado Aquitard

The bottom of Colorado Group (Joli Fou Formation) to the top of Lea Park Shale Formation forms a continuous aquitard with a thickness of more than 600 meters at the study area [3]. This aquitard is usually identified as the Colorado Aquitard. Within this aquitard, the oil-saturated Cardium Sandstone Formation is sandwiched by thick shale layers that have trapped oil in the sandstone formation and should be ideal for use as potential containment sink for CO_2 injection.

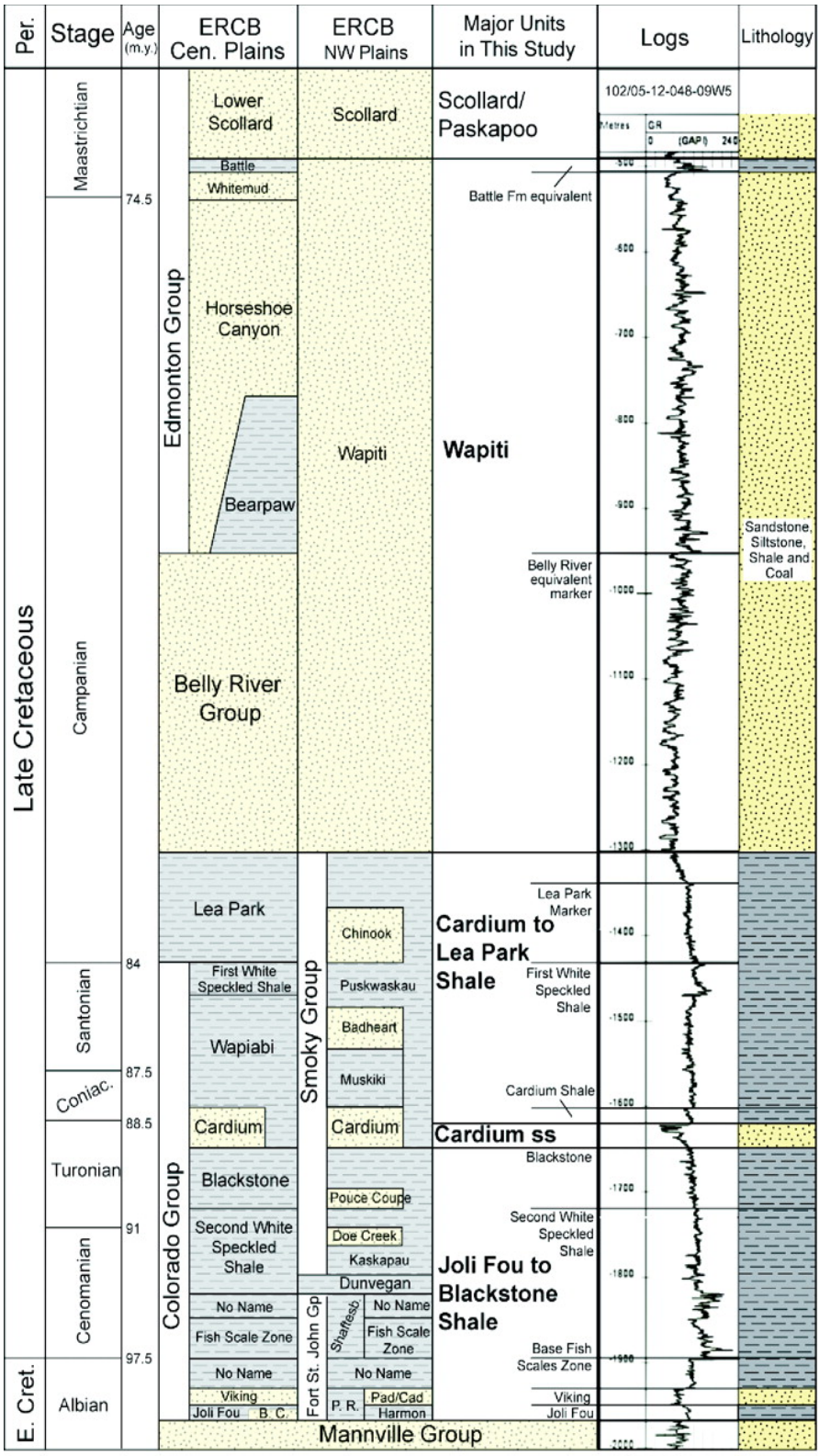

Figure 4-2 Stratigraphic information at Pembina Cardium Field (from Dashtgard et al, 2008)

4.2 Sample Origin - Lea Park Formation

Lea Park Formation shale samples from Well 7-11-48-9W5 were used throughout this research project. A photograph of the Lea Park shale sample that was the source of the test specimens in this study is illustrated in Figure 4-3. Routine geotechnical property measurements, scanning electron microscope (SEM) imaging, energy-dispersive X-ray spectroscopy (EDS) scanning and X-ray diffraction (XRD) analysis were performed on the Lea Park sample.

Figure 4-3 Lea Park shale sample photograph

4.2.1 Geotechnical Index

Routine geotechnical characterization was completed on a Lea Park shale sample from the same well. Table 4-1 show the geotechnical index of Lea Park shale samples.

Table 4-1 Geotechnical properties of Lea Park shale

Depth (m)	G_S	w_L (%)	w_P (%)	I_P	w (%)	e_0
1598.23	2.76	22.0	13.6	8.4	4.4	0.123

where: G_s is specific gravity;

w_L is the liquid limit[%];

w_P is the plastic limit[%];

I_P is the plastic index;

w is the moisture content[%]; and

e_0 is the void ratio.

4.2.2 Scanning Electron Microscope (SEM)

Scanning electron microscopy (SEM) was performed on Lea Park samples by SEM lab at University of Alberta using a JOEL 6301F field emission scanning electron microscope and Zeiss EVO Lab 6 emission scanning electron microscope. All the samples were chromium coated with an Edwards Xenosput XE 200 coater before imaging. Figures 4-4 and 4-5 present results from the SEM imaging. SEM imaging indicates that the Lea Park Shale is highly argillaceous; also, small pores are observed in SEM images.

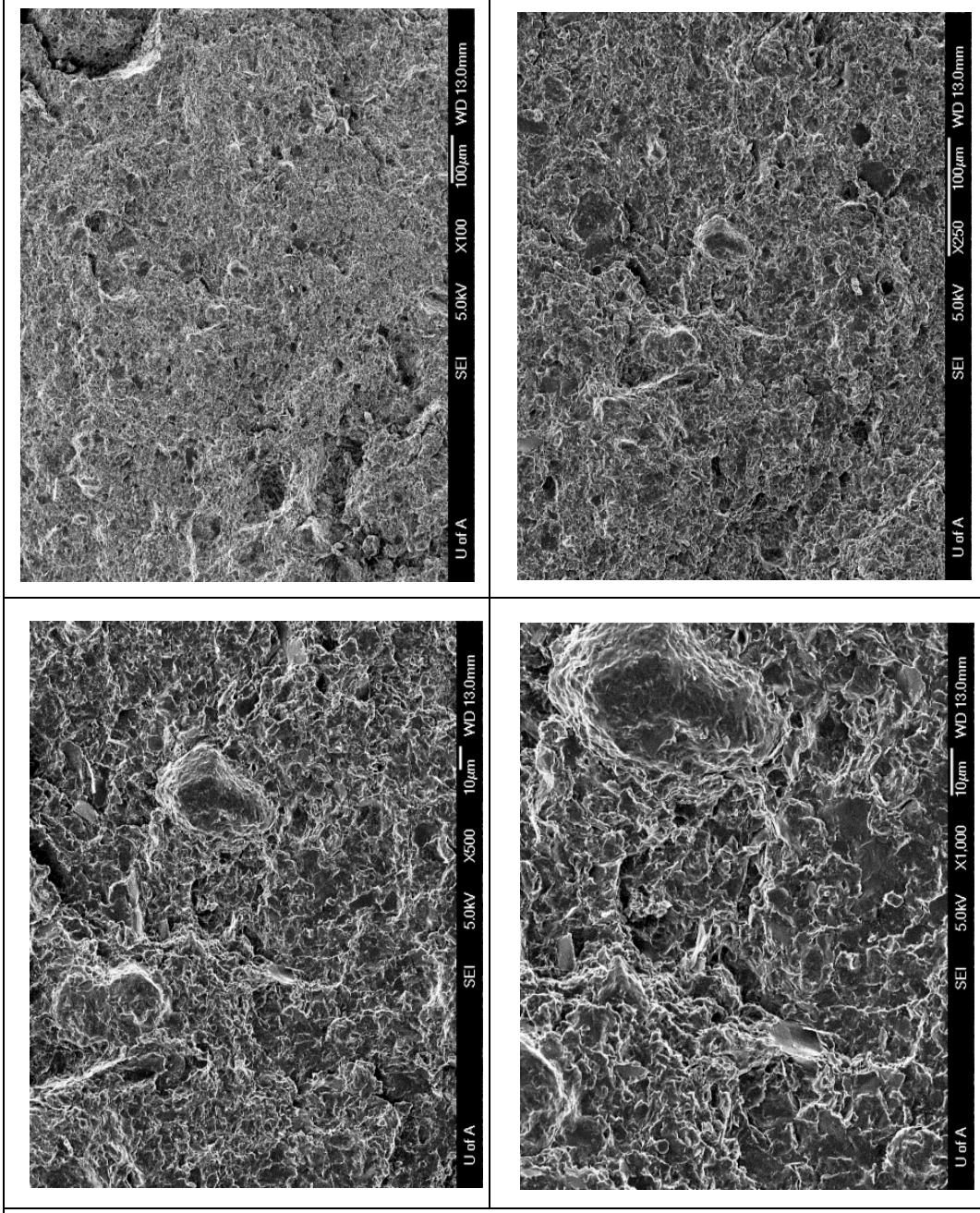

Figure 4-4 SEM images for intact Lea Park shale specimen

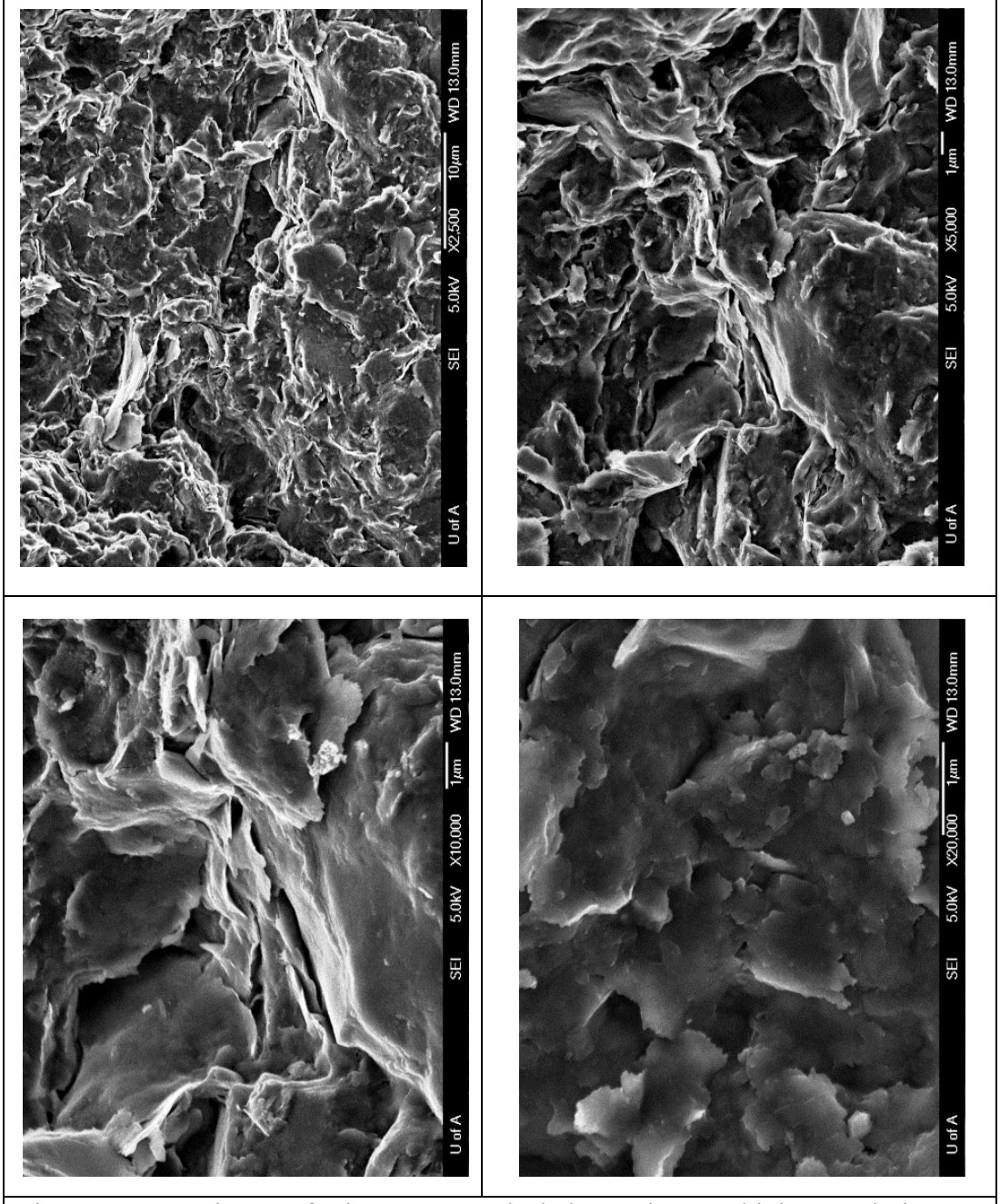

Figure 4-5 SEM images for intact Lea Park shale specimen at higher resolution

4.2.3 Energy-dispersive X-ray Spectroscopy (EDS)

Along with SEM, Energy-dispersive X-ray Spectroscopy (EDS) detection was also performed on Lea Park shale to determine the element compositions using

the same machine. Due to the limitation of equipment, carbon concentration is not available. In total, five scans were conducted at different positions on sample surface and the results were shown in Table 4-2.

Table 4-2 Element concentrations for intact shale sample using EDS

Element	Weight concentration (%)					
	Position1	Position2	Position3	Position4	Position5	Average
Na	1.05	0.19	0.32	0.32	0.49	0.47
Mg	0.40	0.65	1.04	0.94	0.85	0.78
Al	12.13	11.92	10.38	12.28	11.69	11.68
Si	31.64	31.30	32.61	31.04	30.84	31.49
K	2.92	3.10	3.52	3.26	3.26	3.21
Ca	0.23	0.05	0.35	0.37	0.28	0.26
Fe	2.70	4.18	2.91	3.08	4.32	3.44
O	48.93	48.61	48.87	48.71	48.27	48.68

4.2.4 X-ray Diffraction (XRD)

In order to get detail and accurate information on mineralogy (since mineralogy information is not feasible by XPS and EDS), AGAT Laboratories, Calgary, conducted one X-ray Diffraction (XRD) on Lea Park Shale samples at depth of 1598.36m. For clay fraction, sample was first treated in an ultrasonic bath using sodium metaphosphate as a deflocculating agent. Then, materials were centrifuged at different speeds to separate clay fraction from the bulk materials.

The combined bulk and clay XRD results indicate that this Lea Park Formation shale sample consists mainly of quartz, illite, chlorite, kaolinite, plagioclase

feldspar and mixed layer clays (illite-smectite) and the weight fraction (< 3μm) of clay is 30.6% of the total rock volume. XRD results reveal that the illite, chlorite, kaolinite, quartz and mixed layer clays compose the clay matrix at 54%, 21%, 17%, 6% and 1% respectively.

Previous study has also conduct XRD on Lea Park Formation Shale from Weyburn Field, Saskatchewan [13]. The results together with analysis from this research were illustrated in table 4-3 and 4-4.

Table 4-3 Bulk XRD results for Lea Park sample

Component	Weight Percentage (%)	
	From Larsen (2011)	This Research
Quartz	59.8	60.0
Plagioclase	6.3	2.0
K-Feldspar	4.1	N/A
Anhydrite	1.4	N/A
Pyrite	2.0	N/A
Calcite	2.8	N/A
Dolomite	3.0	N/A
Kaolinite	10.0	6.0
Illite	9.2	22.0
Chlorite	1.4	10.0
Smectite	Present	N/A
Mixed layer clay (I-S)	N/A	N/A

Table 4-4 Clay fraction XRD results for Lea Park sample

Component	Weight Percentage (%)	
	From Larsen (2011)	This Research
Quartz	N/A	6.0
Kaolinite	32.8	17.0
Illite	30.4	54
Chlorite	11.0	21
Smectite	25.8	N/A
Mixed layer clay (I-S)	N/A	2.0

Based on XRD results, Lea Park Formation Shale used in this research is a clay-rich material. It is found that compared to Larsen's results, Lea Park Shale in Pembina Field has less carbonate and more clay fraction. So carbonate dissolution/re-precipitation and K-feldspar dissolution are expected to be less important while clay mineral alternation as well as precipitation might be potentially more dominating for Lea Park Shale when exposure to CO_2 in Pembina field.

4.3 Chapter Summary

Lea Park Shale from Pembina Cardium oil field is selected as caprock material. Its mineralogy is analyzed by XRD. Chemistry compositions and structures on shale surface are investigated with EDS and SEM. It is found out that Lea Park shale is highly argillaceous and consists mainly of quartz, illite, chlorite, kaolinite and plagioclase feldspar.

4.4 Reference

1. Lakeman, B., W. Gunter, S. Bachu, R. Chalaturnyk, D. Lawton, D. Everdingen, G. Lim and E. Perkins, 2009. Advancing the deployment of CO_2 monitoring technologies through the Pembina Cardium CO_2 Monitoring Project. Energy Procedia, Vol. 1, pp. 2293-2300.

2. Dashtgard, S., M. Buschkuehle, H. Berhane and B. Fairgrieve, 2008. Geological characterization and potential for carbon dioxide (CO_2) enhanced oil recovery in the Cardium Formation, central Pembina Field, Alberta. Bulletin of Canadian Petroleum Geology, Vol. 56, pp. 147-164.

3. Hitchon, B., 2009. Pembina Cardium CO_2 Monitoring Pilot: A CO_2-EOR PROJECT, ALBERTA, CANADA: Final Report, 392p.

4. Shevalier, M., M. Nightingale, G. Johnson, B. Mayer, E. Perkins and I. Hutcheon, 2009. Monitoring the reservoir geochemistry of the Pembina Cardium CO_2 Monitoring Project, Drayton Valley, Alberta. Energy Procedia, Vol. 1, pp. 2095-2102.

5. Lawton, D., A. Alshuhail, M. Coueslan and L. Chabot, 2009. Pembina Cardium CO_2 Monitoring Project, Alberta, Canada: Timelapse seismic analysis-lessons learned. Energy Procedia, Vol. 1, pp. 2235-2242.

6. Krause, F., K. Deutsch, S. Joiner, J. Barclay, R. Hall, L. Hills, 1994. Cretaceous Cardium Formation of the Western Canada Sedimentary Basin. Geological Atlas of the Western Canada Sedimentary Basin. G.D. Mossop and I. Shetson (eds). Alberta Research Council and Canadian Society of Petroleum Geologists, pp. 365-385.

7. Bachu, S. and S. Stewart, 2002. Geological sequestration of anthropogenic carbon dioxide in the western Canada Sedimentary Basin: Solubility Analysis. Journal of Canadian Petroleum Technology, Vol. 41, No. 2, pp. 32-40.

8. Law, D. and S. Bachu, 1996. Hydrogeological and numerical analysis of CO_2 disposal in deep aquifers in the Alberta sedimentary basin. Energy Conversion and Management, Vol. 37, pp. 1167-1174.

9. Michael, K., S. Bachu and H. Machel, 2000. Groundwater flow in response to ground surface topography, erosional rebound, and hydrocarbon generation in Cretaceous strata in the Alberta Basin, Canada. Journal of Geochemical Exploration, Vol. 69-70, 657-661.

10. Bachu, S., M. Brulotte, M. Brobe and S. Stewart, 2000. Suitability of the Alberta Subsurface for Carbon-Dioxide Sequestration in Geological Media. Earth Sciences Report, Alberta Research Council, Edmonton, AB, Canada, 86 pp.

11. ASTM D4643-08. Standard Test Method for Determination for Water (Moisture) Content of Soil by Microwave Oven Heating.

12. ASTM D4318-10. Standard Test Methods for Liquid Limit, Plastic Limit, and Plastic Index of Soils.

13. Larson, A., 2011. Laboratory Investigation of the Sealing Properties of the Lea Park Shale with Respect to Carbon Dioxide. M.Sc Thesis, University of Calgary. 126 p.

5 Experimental Design and Procedures

This chapter discusses the experimental design and procedures for this research and provides the results from the cell reaction tests and the capillary entry pressure and permeability measurements carried out to investigate caprock/brine/CO_2 interactions and caprock sealing integrity. Chemical composition information was primarily investigated using XPS scanning. In XPS (X-ray Photoelectron Spectroscopy), also known as ESCA (Electron Spectroscopy for Chemical Analysis), the sample is irradiated with X-rays, which leads to emission of photoelectrons from sample surface. The binding energy of electrons is recorded by an electron analyzer. Quantity of an element is then able to be determined from the binding energy and intensity. Surface structure was analyzed using SEM with the addition of EDS to generate additional data about chemical composition (since XPS can only measure the chemical composition of the top 2μm while EDS can penetration into 30μm). Capillary entry pressure and permeability measurements were conducted in a specialized cell within GeoREF.

5.1 Cell Reaction Test

In order to model and investigate caprock/brine/CO_2 interactions, a cell reaction test was designed. In total, two rock/brine/compressed air blank tests and five rock/brine/CO_2 reaction tests were conducted using the same test system.

5.2 Plastic holding system

Due to the sample size requirement of XPS scanning, very tiny shale caprock chips had to be used in this test programme. A consequent problem associated with small shale rock sample was disintegration (Figure 5-1).

Figure 5-1 Disintegration of shale samples after 48 hours

In order to prevent sample disintegration and collapse, a special plastic holding system was designed to protect shale samples. Acrylic plastic and epoxy resin were selected finally since they are non-reactive when exposed to CO_2 rich brine, thus won't affect chemical reaction test result. Its design is illustrated in Figure 5-2 and 5-3.

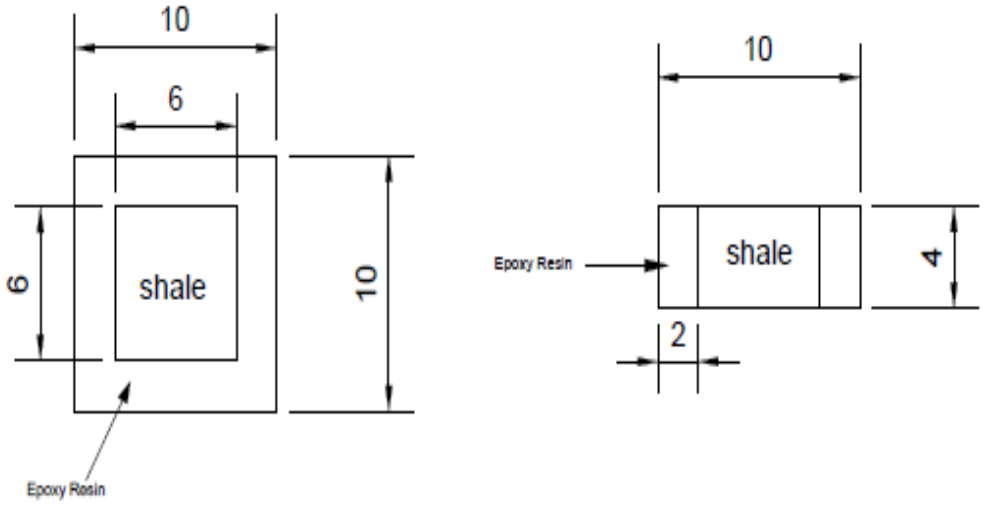

Figure 5-2 Dimensions of plastic holding system (Unit: mm)

Figure 5-3 Picture of plastic held test specimens

5.2.1 Sampling Procedures

Procedures for sampling in this cell reaction test are:

1. Cut 5mm thickness hard plastic sheet into small cubes with dimensions of 1 cm^2 at top. Clean and dry them.
2. Drill a hole at the centre of every plastic cube using electrical drill and make sure the no tube is pierced through. Blow out all the remaining materials in the hole using compressed air blower.
3. Crush rock cores and choose small pieces that fall from the core, being careful not to touch any piece with fingers.
4. Fill the hole with epoxy resin, slide rock chip into the hole, be careful don't contaminate sample surface with epoxy resin. Don't trim the sample surface to keep the structure undisturbed.
5. Let epoxy resin cure overnight in moisture room so they are strong enough to hold the rock chip.

5.2.2 Cell Reaction Test Apparatus

Schematic of the testing systems are illustrated in Figures 5-4 and 5-5. The test system is comprised of three main elements:

- A saturation system which includes a cell, a pressure source with pressure controlling and monitoring system.
- A reaction system consists of cell, a pressure source with pressure control and monitor system and a temperature control and monitor system.
- Two reservoir systems to prevent back flushing of brine into air bottle.

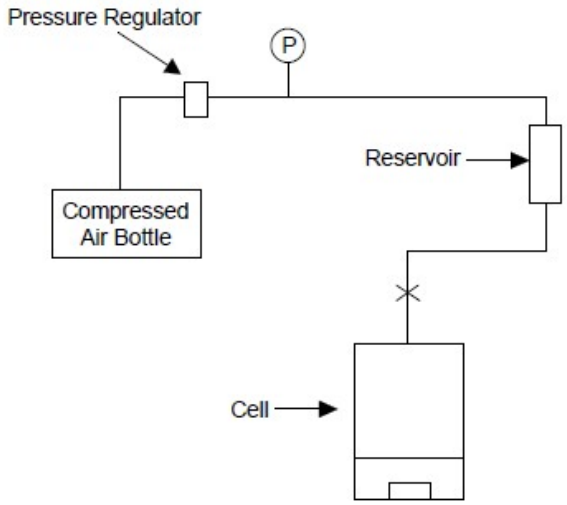

Figure 5-4 Saturation cell system

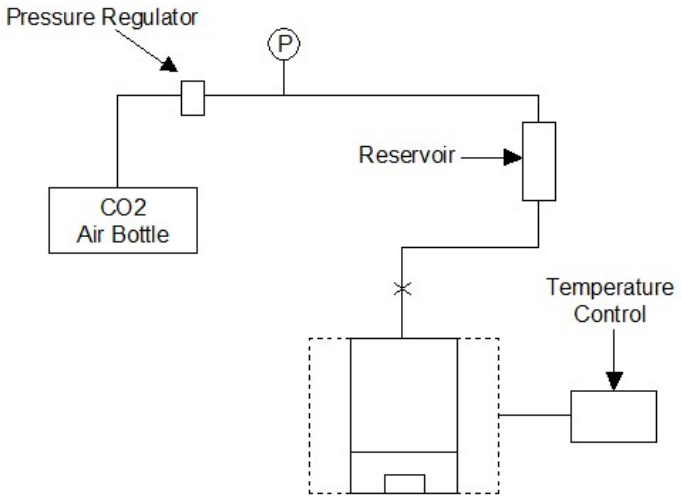

Figure 5-5 Reaction cell system

5.2.3 Pore Fluid

Due to the lack of in situ water sample, 3g/L NaCl solution was selected to model in situ formation brine.

5.3 Capillary Breakthrough Test

Capillary breakthrough test was carried out to evaluate the capillary sealing integrity of Lea Park Shale.

5.3.1 Sampling

Sample preparation was one of the biggest challenges throughout this research project since Lea Park shale is an extreme fragile material. Initially, a rock saw was selected to cut the sample to proper length of around 2 inch and then use cutting ring trying to get 2.5 inch sample. However, the rock saw did not work effectively when cutting due to sample brittleness. The saw-cutting resulted in either breaks in the sample or introduced serious damage to the sample surface. A second attempt was made by placing the shale sample in a paper box and then filling it with plaster of Paris, which acted as a confining material and provide lateral support to rock core. The box was subsequently mounted in a coring machine and a 2.5 inch core barrel was used to drill through the sample. During the whole process, a small amount of water was used as circulated fluid (Figure 5-6). However, in all five attempts, the material crumbled. A later decision to replace water circulation with air circulation led to same result.

Through these failed sample preparation attempts, the initial sample of Lea Park shale was destroyed and so an additional sample of Lea Park shale was selected

from a nearby well, Well 4-11-49-8W5. Ultimately, a decision was made to prepare the samples manually. The rock samples were placed and confined in plaster of Paris to create a smooth base surface, a 2.5 inch cutting ring was placed on top of sample, and then sample was trimmed by a very sharp knife with extreme care. A small amount of silicon oil was spread on the sample surface and cutting ring blade to prevent desiccation and act as lubricant as well. All the work was conducted in a room with constant temperature (4°C) and moisture (90%). Two relative good quality samples were prepared after 4 hours of trimming each. The average dimensions of two samples were presented in Table 5-1 and their photos are illustrated in Figures 5-7 and 5-8. It was noted that this shale material contained a substantial number of small visible fissures, which might results in high permeability and low capillary entry pressure values (Figure 5-9).

Another problem associated with tests using CO_2 is the membrane, which for traditional geotechnical testing is latex rubber. Unfortunately, CO_2 can diffuse through latex very quickly. Consequently, in the final test procedure, a lead sleeve was used as a membrane. The prepared specimen is placed on the bottom pedestal that has a saturated porous stone on it. The sample is then wrapped with a lead sleeve and an additional Viton membrane is placed outside of the lead sleeve. At last, a second saturated porous stone is placed on the top of the specimen followed by the top pedestal and the membranes are sealed to the pedestals using two host champs.

Table 5-1 Sample dimensions for capillary and permeability measurements

Sample No.	Depth (m)	Diameter (mm)	Height (mm)
LP1	1530.75-1531.02	60.10	26.70
LP2	1532.80-1532.98	65.21	26.70

a)  b) 

Figure 5-6 Shale specimen preparation. a) samples in plaster of Paris and b) coring machine

 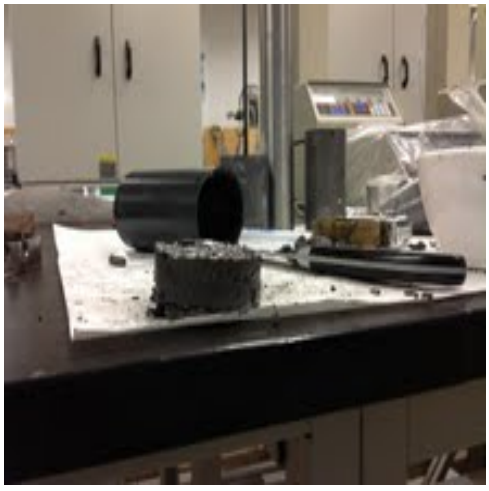

Figure 5-7 Testing sample LP1

Figure 5-8 Testing sample LP2

Unexpected leakage was observed in the initial trial tests. After inspection, it was concluded that during consolidation, the sampled underwent contraction which led to a decrease in both sample height and diameter. As mentioned above, the specimen is sandwiched between the top and bottom pedestals with two saturated porous stones, since the pedestals are much stiffer than the shale specimen when subject to high confining pressure, at the interface between shale specimen and stainless dispenser; the lead sleeve is sheared due to uneven displacement. Once the differential displacement reaches a critical point, the lead sleeve breaks and is no longer able to seal the sample and consequent leakage occurs.

In order to maintain integrity of the seal system, an extra thin layer of patching was applied to the side of the test specimen to minimize the differential displacement, thus reduce the shear generated at the interface. No leakage was observed following this modification.

Figure 5-9 Fissures in Lea Park shale core

Figure 5-10 Failure of lead sleeve (bottom left)

5.3.2 In Situ Stress

Based on the final report of Pembina Cardium CO_2 Monitoring Pilot Project, the average horizontal stress in the PennWest field is 18.5 kPa/m in the caprock. The range of corresponding confining stress for the core sample was 28.32 MPa to 25.36 MPa. Assuming hydrostatic conditions from ground level, the calculated pore pressure is between 15.02 MPa and 15.04 MPa. Based on these values, the confining pressure and pore pressure chosen for this research were set at 28.5 and 15.0 MPa, respectively.

5.3.3 Capillary Breakthrough Test Apparatus

A complex test system was designed to measure capillary entry pressure and permeability of Lea Park Shale. Test station is illustrated in Figures 5-11 to 5-13. Silicon oil was selected to apply confining pressure and 3g/L NaCl was used to as pore fluid. The complete test apparatus was placed in the LBB 2-27-1 oven. The oven temperature was set to 50°C and the temperature limit was programmed to be 65°C so the heater would automatically shut off when the temperature exceeds this limit. 3 ISCO pumps (A,B,C in Figure 5-11) were used to apply pressure, in addition, 3 Honey Well FPG pressure transducers and 1 VALIDYNE DP15-TL differential pressure transducer (rectangular in Figure 5-11) were included in the systems to collect extra pressure data besides pump data. Compressed air was used to drive the fluid.

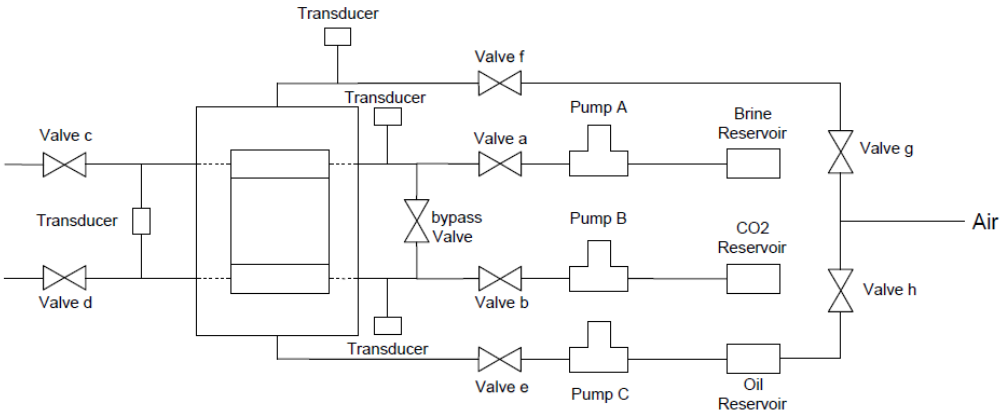

Figure 5-11 Test station for capillary entrance pressure and permeability measurements

5.3.4 Leak Test

After the testing system construction was finished and prior to introducing any fluid into the system, a leak test was conducted using compressed air under the pressure of 1MPa to check system leakage - no leakage was detected. This procedure was repeated before doing any test on this station to ensure the accuracy of data and the calculated results.

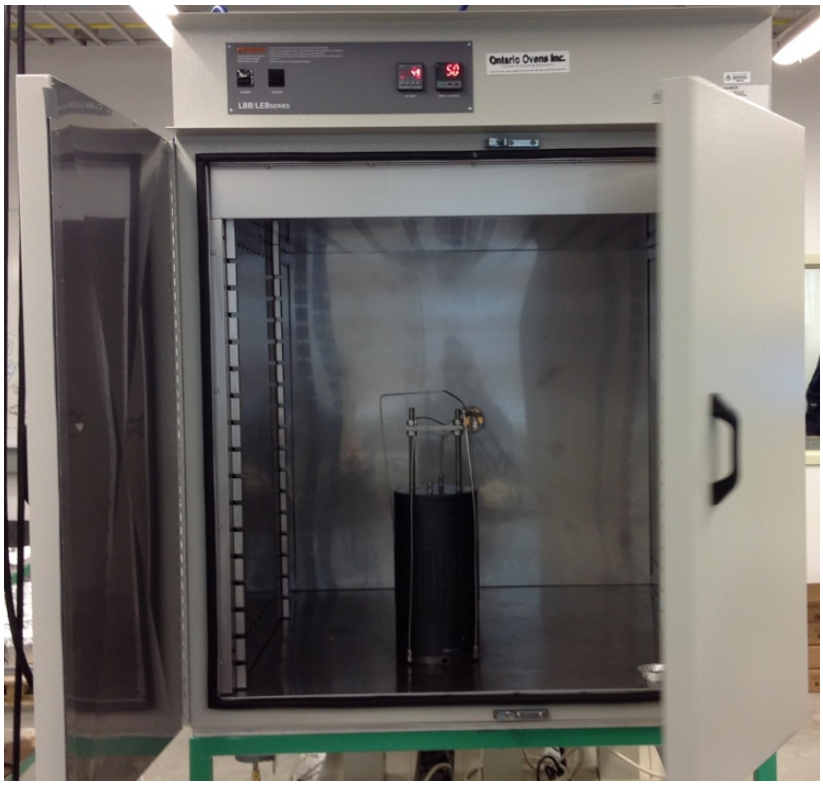

Figure 5-12 Test station (Front View)

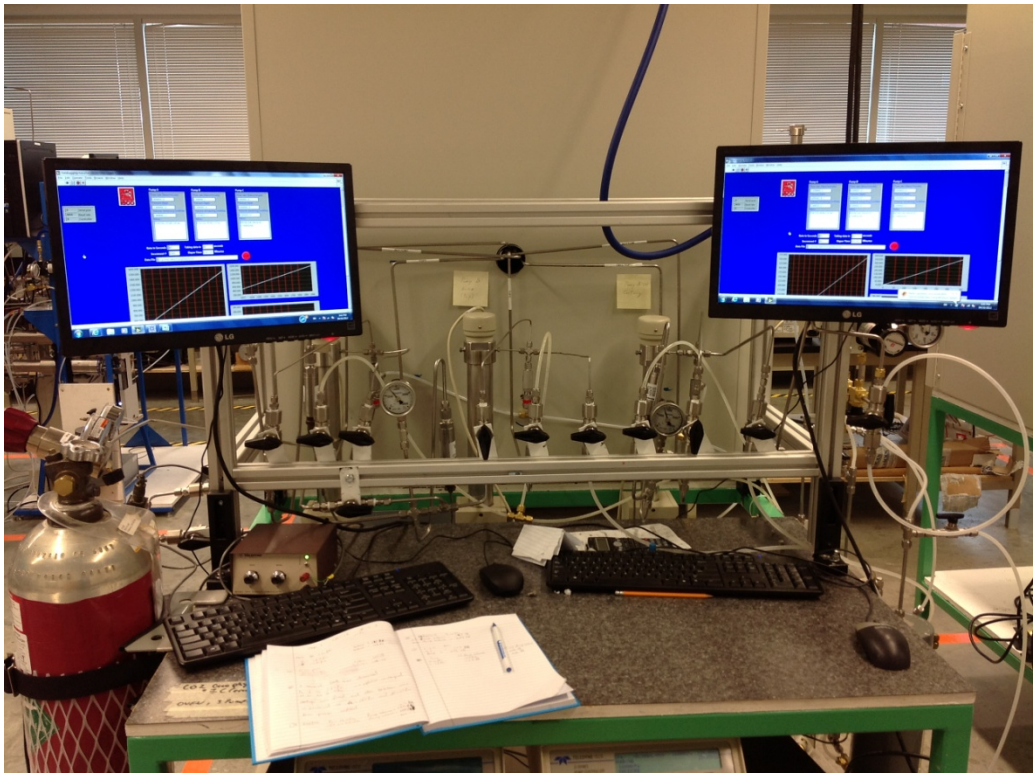

Figure 5-13 Test station (Rear view)

5.3.5 Measurement of Reservoir Volumes and Compressive Storage

In order to calculate permeability using the pulse-decay method, reservoir volumes and compressive storage need to be measured experimentally. Since changes in confining pressure will significantly affect the result, confining pressure was set at 10MPa and remained constant during all the measurements.

Using Figure 5-11 as a reference, the following provides the procedure for reservoir volume and system compressibility measurements. To measure the upstream reservoir volume, open valve "a" and "c" and set pump B at constant flow rate until no air bubbles are observed at "c". No air bubble signifies that the upstream system is saturated with synthetic pore fluid. N_2 is then introduced into the system to displace the fluid and all the replaced fluid was collected in a graduated cylinder and its volume is measured. This process was repeated 3 times and the average value is used in the calculation. For the downstream volume, since it is not possible for direct measurement, both reservoirs were saturated with synthetic pore fluid by opening valves "a", "bypass", "b" and "d" followed by its displacement with air. Again using the same method, the total system volume is measured. The downstream volume will then be the difference between total volume and upstream volume. The average values of both reservoir volumes were 60.2 ± 0.3 and 75.6 ± 0.3 mL, respectively.

For reservoir compressive storage measurement, an aluminum plug was selected as "dummy sample" and was considered as an impermeable material. Both reservoirs were saturated with synthetic pore fluid prior to test. Cell pressure was set at 10MPa before the test to minimize the impact of reservoir compression due

to change of cell pressure. Since a pump was connected to the system, it was not possible to directly measure the compressive storage of an individual reservoir. In order to undertake the measurement, all valves were closed initially and the pump volume V_0 was recorded. After that, pump "A" pressure was set to a pre-designed value P and after the pressure was stable, the pump volume V_1 was recorded, then, valve "a" was opened and pump volume V_2 was recorded when pressure reading is stable, at last, bypass valve was opened and pump volume of V_3 was recorded. As a result, $(V_1 - V_0)$, $(V_2 - V_1)$ and $(V_3 - V_2)$ will define the compressive storage of pump, upstream reservoir and downstream respectively. The same procedures were conducted over the pressure range from 3 to 6 MPa at 0.25 MPa increment. Figure 5-18 shows the results of reservoir compressive storage for both reservoirs.

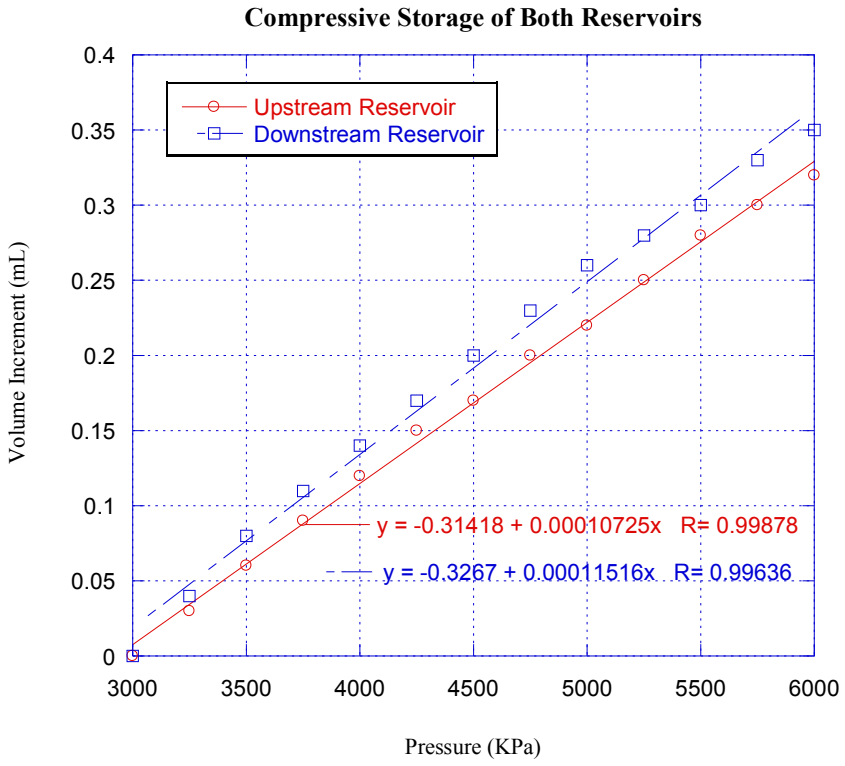

Figure 5-14 Compressive storage measurement results for both reservoirs

The measured results indicated that the upstream reservoir compressive storage is $1.0725*10^{-13} \pm 0.0053*10^{-13}$ and $1.1516*10^{-13} \pm 0.0046*10^{-13}$ m^3/Pa, respectively.

5.3.6 Saturation

After mounting the clay shale sample within the test cell and assembling the entire system, saturation of the specimen is the next important step in the test procedure. This is achieved by opening valve "a", "bypass" and "b". Confining and backpressures were set at 5.1MPa and 5MPa, respectively for overnight. A B test was then conducted to calculate the saturation of testing specimen. The same procedures were repeated until degree of saturation exceeds 95%. In addition, the backpressure pump volume is also monitored to ensure it remains constant. Since most of the system is inside the oven and could be considered as isothermal condition, if the pump volume keeps constant, it is also considered that the sample is fully saturated.

5.3.7 Consolidation

Following saturation but prior to permeability and capillary pressure measurements, the specimen must be consolidated to in-situ stress state. This was achieved by increasing confining stress at different increments until 28.5 MPa while keeping backpressure constant at 15 MPa. Table 5-2 shows the pressure increment arrangement for consolidation. In each stage, the specimen is left to consolidate for 24 hours.

Table 5-2 Pressure increment during consolidation process

Stage	Confining Pressure (MPa)	Back Pressure (MPa)
1	16	15
2	17	15
3	19	15
4	23	15
5	28.5	15

5.4 Permeability Measurement

Permeability measurements were conducted on the shale specimen using the pulse decay method prior to performing capillary entry pressure measurements.

5.5 Chapter Summary

Batch reaction tests were adopted for chemical reaction. Due to the nature of disintegration, a plastic holding system was designed to confine shale sample so it could be soaked in brine during test duration. On the other hands, a test station was designed and constructed for permeability and capillary pressure measurements.

6 Test Results and Analysis

In this chapter, chemical composition from the cell reaction test determined using XPS scanning, SEM imaging and EDS analysis as well as the specimen threshold pressure and permeability from capillary breakthrough test and permeability measurement results are presented and analyzed.

6.1 Cell Reaction Test

Five cell reaction tests using CO_2 were carried out. Chemical composition information was investigated using XPS scanning. Surface structure was determined using SEM and EDS was also conducted during SEM to generate extra information on chemical composition. Two parallel blank tests using compressed air instead of CO_2 were performed separately at same test conditions for comparison.

6.1.1 X-ray Photoelectron Spectroscopy (XPS)

Two parallel blank tests using compressed air were conducted with XPS scanning both prior to and after interaction. Table 6-1 shows the result of blank tests using compressed air.

From the blank tests, following changes were observed:

- Slight increase for both samples in Na, this is probably due to the left-over NaCl in pores.
- Moderate to high increase in Fe, 30.93% for Sample A and 77.18% for Sample B.

- Decrease in Si and Al for Sample A compared with almost unchanged and increase in Sample B indicates sample heterogeneity.

Table 6-1 Weight concentration from blank test (Unit :%)

Sample	Sample A (216hrs)		Sample B (1008hrs)	
	Intact	End of test	Intact	End of test
Na	0.70	0.93	0.69	0.98
Fe	1.81	2.37	1.49	2.64
O	47.54	48.55	49.71	47.20
N	0.77	0.62	0.97	0.42
Ca	0.57	0.47	0.80	0.58
K	3.52	2.97	3.81	3.77
C	9.09	9.36	8.59	8.27
Si	22.48	19.18	22.91	22.30
Al	13.51	12.80	11.03	13.84

Besides blank tests, five cell reaction tests using CO_2 were carried out. Changes in element weight concentration for each test sample are presented below in Tables 6-2 to 6-6.

Table 6-2 Element weight concentration for Sample No.1 with reaction time of 48 hours (Unit: %)

	Na	Fe	O	N	Ca	K	C	Si	Al
Intact	0.42	1.39	41.66	1.91	0.63	2.55	20.02	19.37	12.06
Exposed	0.11	2.12	41.43	2.46	0.59	2.47	19.26	19.99	11.58

Table 6-3 Element weight concentration for Sample No.2 with reaction time of 216 hours (Unit: %)

	Na	Fe	O	N	Ca	K	C	Si	Al
Intact	0.40	1.12	41.42	2.20	1.10	1.49	25.98	16.20	10.11
Exposed	0.09	0.75	39.28	2.80	0.35	1.60	28.59	17.43	9.12

Table 6-4 Element weight concentration for Sample No.3 with reaction time of 384 hours (Unit: %)

	Na	Fe	O	N	Ca	K	C	Si	Al
Intact	0.16	1.59	42.08	1.40	0.38	2.56	18.79	19.92	12.18
Exposed	0.10	1.41	36.79	2.03	0.42	1.52	28.02	19.68	10.04

Table 6-5 Element weight concentration for Sample No.4 with reaction time of 552 hours (Unit: %)

	Na	Fe	O	N	Ca	K	C	Si	Al
Intact	0.35	1.63	45.90	0.80	0.62	3.15	12.32	22.73	12.51
Exposed	0.00	3.02	39.55	3.35	0.78	1.77	27.66	14.73	9.14

Table 6-6 Element weight concentration for Sample No.5 with reaction time of 1008 hours (Unit: %)

	Na	Fe	O	N	Ca	K	C	Si	Al
Intact	0.46	1.10	46.79	0.71	0.71	3.14	11.67	22.61	12.82
Exposed	0.42	2.61	43.00	3.05	0.30	1.52	22.27	17.24	9.60

Figure 6-1 shows the weight concentration change for calcium. The fluctuations in the calcium concentrations provide some evidence for dissolution/precipitation of carbonate reactions occurring with the shale. However, due to the low concentration, heterogeneity between specimens could also be responsible for this variation.

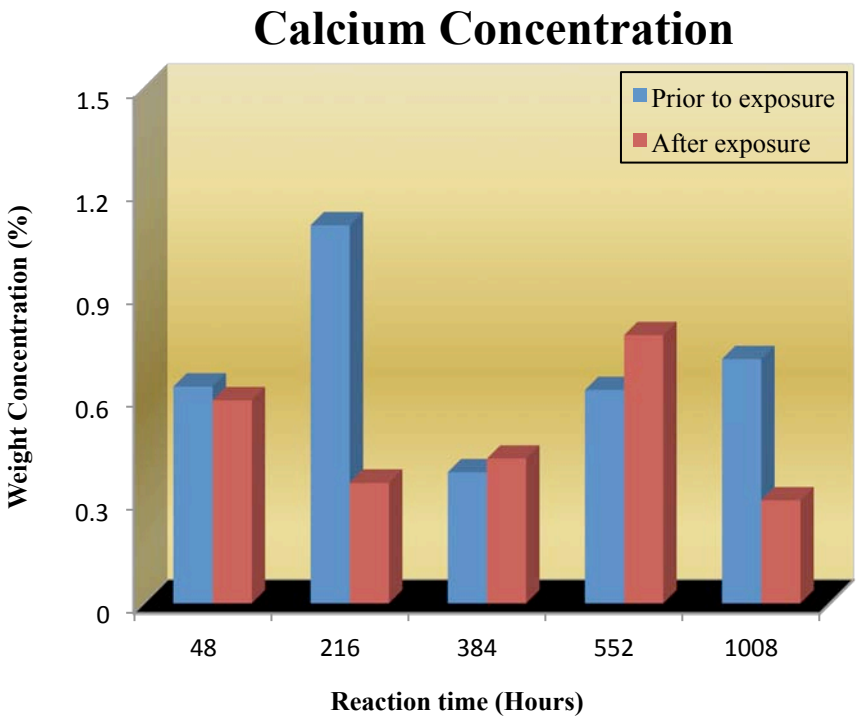

Figure 6-1 Weight concentration change for calcium

Figure 6-2 presents weight concentration changes for potassium. It is observed that the potassium concentration remains constant for a reaction time less than 216 hours but decreases for longer periods of exposure. Based on XRD results, the major source of potassium is illite, so this decrease in potassium concentration is probably introduced by illite ($[KAl_2(OH)_2(AlSi_3(O,OH)_{10})]$) dissolution; this observation is consist with previous studies [15][16].

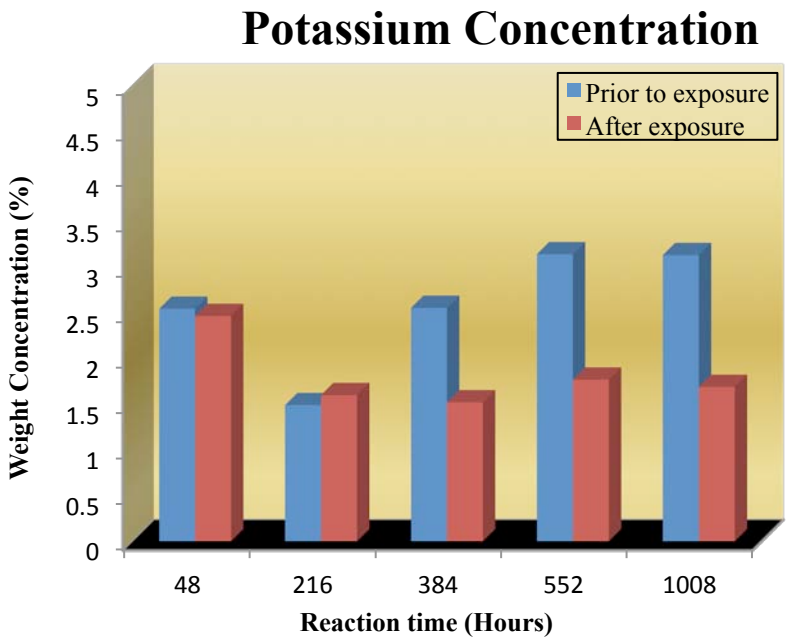

Figure 6-2 Weight concentration change for potassium

Figure 6-3 illustrates weight concentration change for aluminum. All the samples exhibit aluminum loss except for the first two which may simply reflect heterogeneity amongst the specimens. Based on XRD analysis, the decrease in potassium is likely due to the dissolution of illite. Assuming that other minerals in the specimens were non-reactive, it is possible to calculate the impact of illite dissolution on aluminum loss based on potassium loss. The relationship between illite and potassium decrease is expressed as:

$$\frac{\Delta m_i}{\Delta m_K} = \frac{M_i}{M_K} \qquad [4]$$

where: Δm_i is the decrease in illite concentration (%);

Δm_K is the decrease in potassium concentration (%);

M_i is the relative atomic mass of illite; and

M_K is the relative atomic mass of potassium.

The relationship between illite and aluminum loss is shown as:

$$\frac{\Delta m_i}{\Delta m_{Al}} = \frac{M_i}{3M_{Al}} \quad [5]$$

where: Δm_i is the decrease in illite concentration (%);

Δm_{Al} is the decrease in aluminum concentration (%);

M_i is the relative atomic mass of illite; and

M_{Al} is the relative atomic mass of aluminum.

Combining the above two equations, the relationship between aluminum and potassium loss can be expressed as:

$$\frac{\Delta m_K}{\Delta m_{Al}} = \frac{M_K}{3M_{Al}} \quad [6]$$

where: Δm_K is the decrease in potassium concentration (%);

Δm_{Al} is the decrease in aluminum concentration (%);

M_K is the relative atomic mass of potassium; and

M_{Al} is the relative atomic mass of aluminum.

Table 6-7 shows the calculation results compared with actually measurement. It is noticed that the difference between calculated and measured aluminum loss is very small and provides evidence that the potassium and aluminum concentration changes are due to illite dissolution.

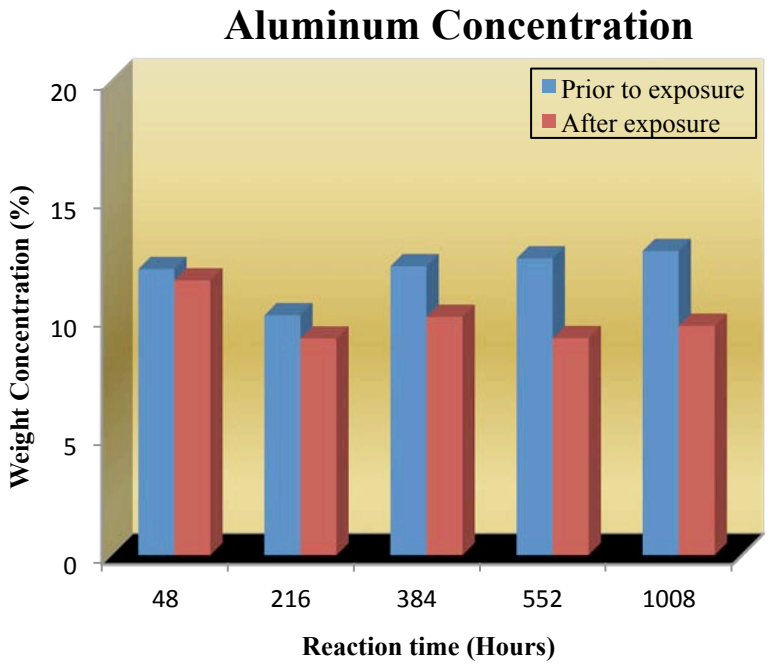

Figure 6-3 Weight concentration change for aluminum

Table 6-7 Comparison between calculated and measured aluminum loss (Unit: %)

	Sample No.3	Sample No.4	Sample No.5
ΔK	1.04	1.38	1.45
ΔAl (calculated)	2.16	2.87	3.01
ΔAl (measured)	2.24	3.37	3.16

Figure 6-4 presents the weight concentration change for carbon. Within the first 48 hours, the carbon concentration remains relatively constant but displays a consistent increase at increasing periods of exposure. The last three specimens which were exposed for 384, 552 and 1008 hours showed increases in carbon of 49.1%, 124.5% and 88.9%, respectively. These changes are likely due to carbon adsorption of the clay minerals within the Lea Park Shale over the experimental period. This adsorption potential is very positive as it will provide an additional storage capacity in the seals in the event there is upward migration of CO_2.

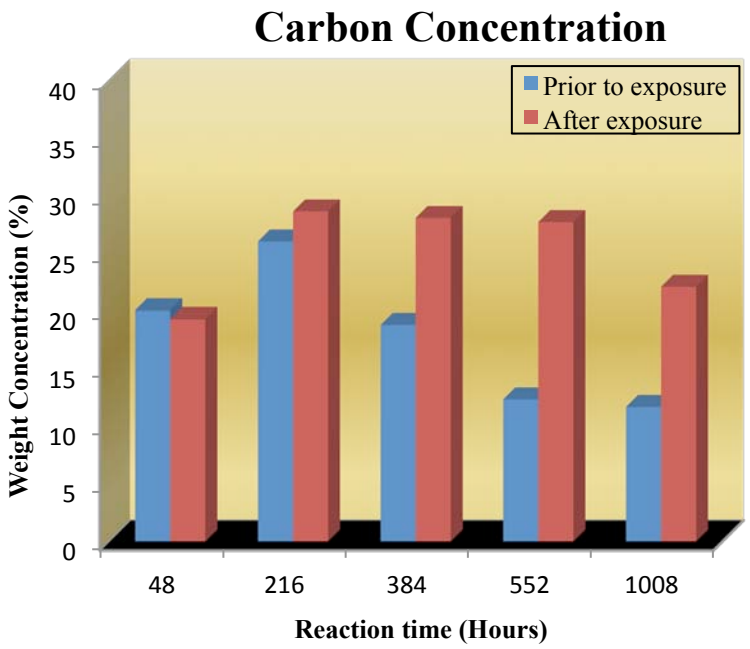

Figure 6-4 Weight concentration change for carbon

The weight concentration change for silicon is illustrated in Figure 6-5. It is observed that within 384 hours the silicon concentration remains almost constant, followed by a decrease with longer exposure time to CO_2-rich brine. This decrease in surface silicon concentration reveals silicon release from Lea Park shale when exposed to CO_2-rich brine.

Figure 6-6 presents the weight concentration change for iron. Its concentration increased at the end of 48 hours, then decreased until the end of 384 hours, followed by another rise until the end of batch reaction test. A possible explanation is as CO_2 dissolves, it acidizes the brine which lead to iron related mineral dissolution and as time increases, precipitation of new iron related minerals eventually increase the iron concentration.

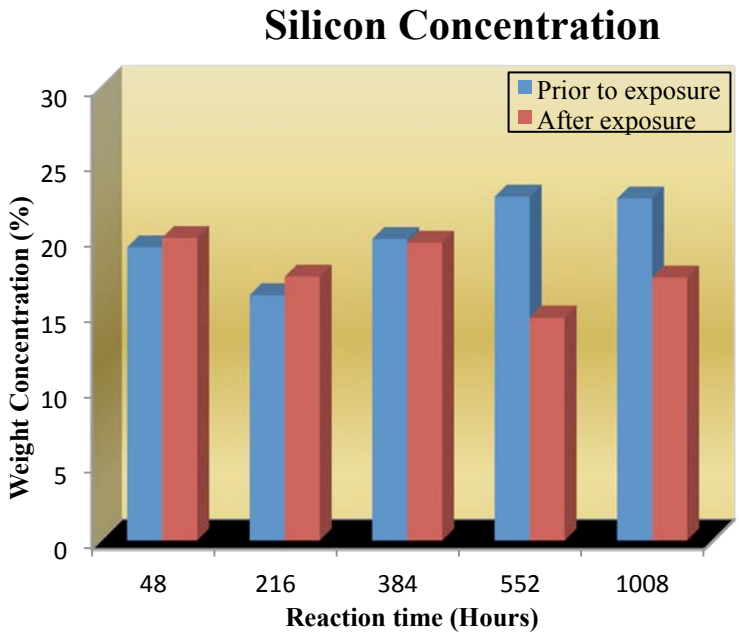

Figure 6-5 Weight concentration change for silicon

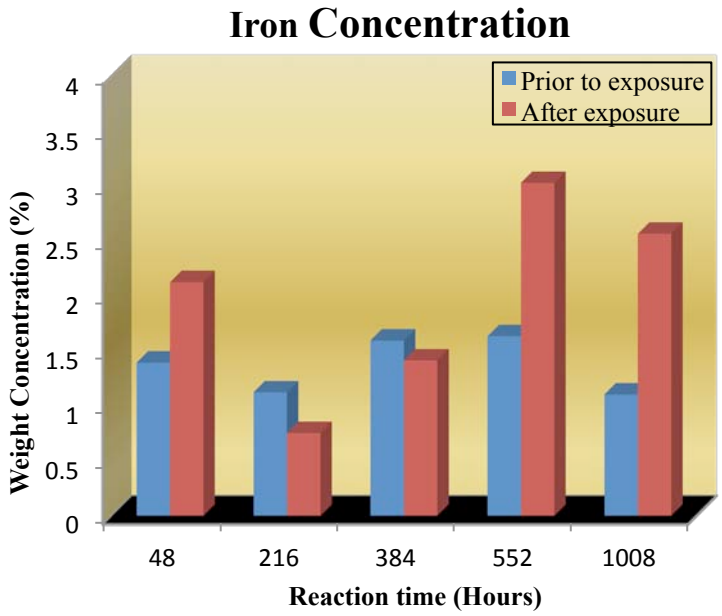

Figure 6-6 Weight concentration change for Iron

It is very interesting to compare the ratio between aluminum and silicon weight concentrations (Table 6-8). It was found that for the first three samples, the Al/Si ratio was decreasing and the reduction was proportional to reaction time, up to

384 hours. However, this ratio began to rebound after that, reaching a peak value at 552 reaction hours and for 1008 hours, the Al/Si ratio is the same for the initial and reacted specimen.

Table 6-8 Ratios between aluminum and silicon weight concentration

Sample No.	Reaction Time (Hours)	Al/Si	
		Intact	Reacted
1	48	0.62	0.57
2	216	0.62	0.52
3	384	0.61	0.51
4	552	0.55	0.62
5	1008	0.56	0.55

6.1.2 Scanning Electron Microscope (SEM)

SEM imaging was used to analyze Lea Park shale surface structure. An intact sample and all the five rock/brine/CO_2 interacted samples were scanned. Figures 6-7 to 6-9 provide the SEM images for all 6 samples under magnifications of 2500X, 5000X and 10000X, respectively. Except for image "d" which displayed at 1000X magnification in Figure 6-7 due to a loss of data.

Specimens a – d were imaged by JOEL 6301F field emission scanning electron microscope while specimens e-f were imaged by a Zeiss EVO Lab 6 emission scanning electron microscope.

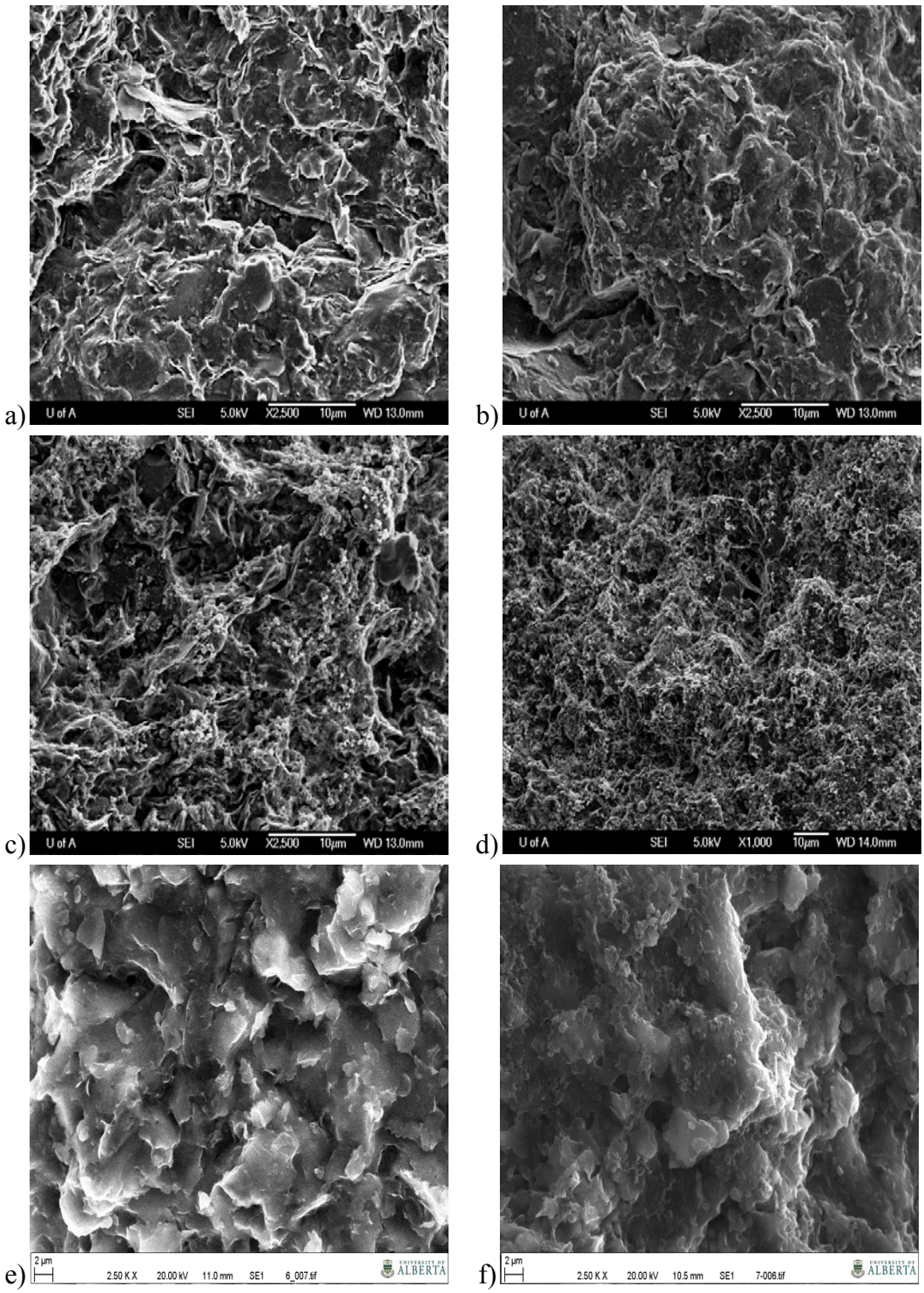

Figure 6-7 SEM images at 2,500X magnification. a) Intact; b) 48 hours; c) 216 hours; d) 384 hours; e) 552 hours and f) 1008 hours

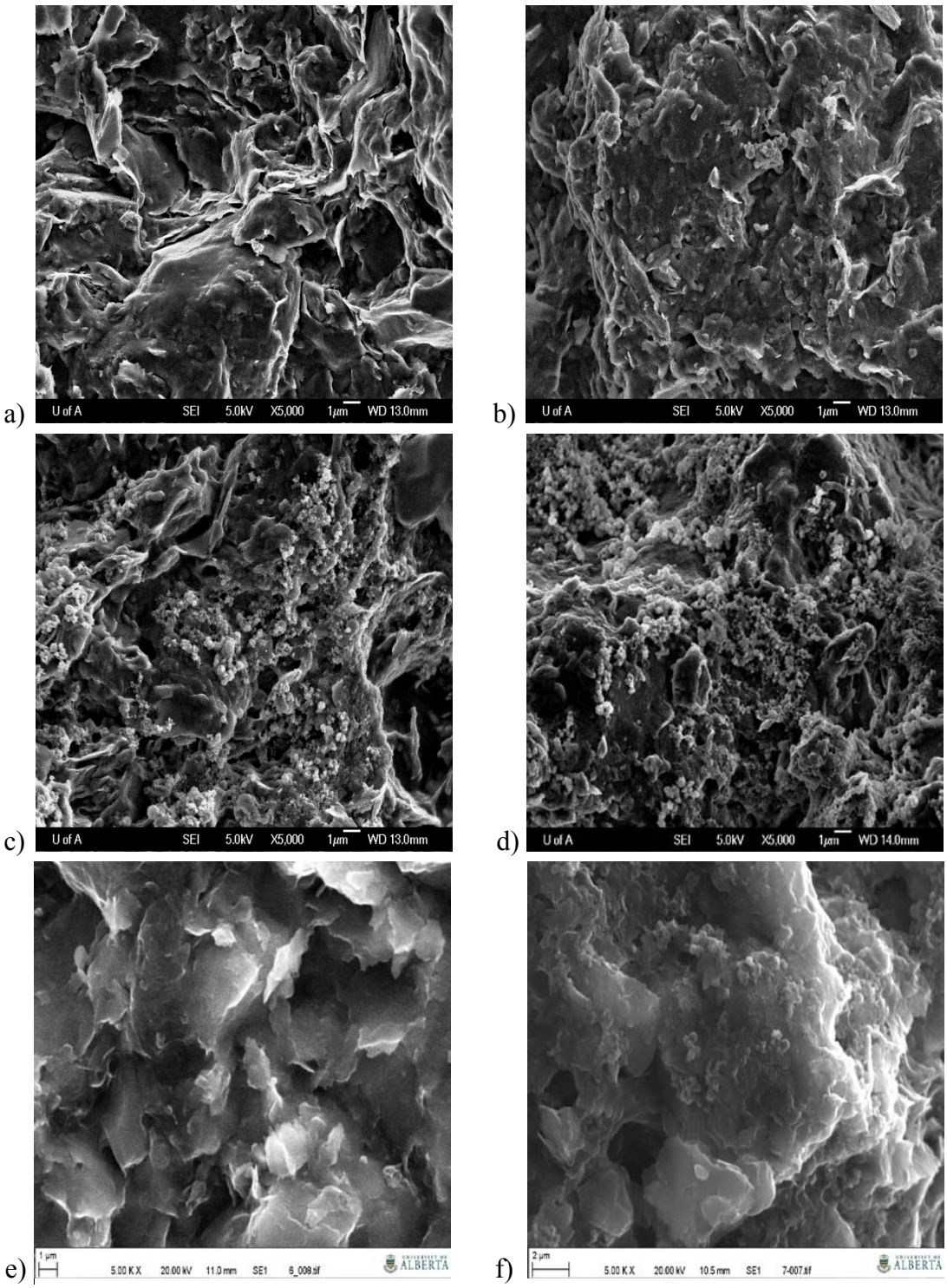

Figure 6-8 SEM images at 5,000X magnification. a) Intact; b) 48 hours; c) 216 hours; d) 384 hours; e) 552 hours and f) 1008 hours

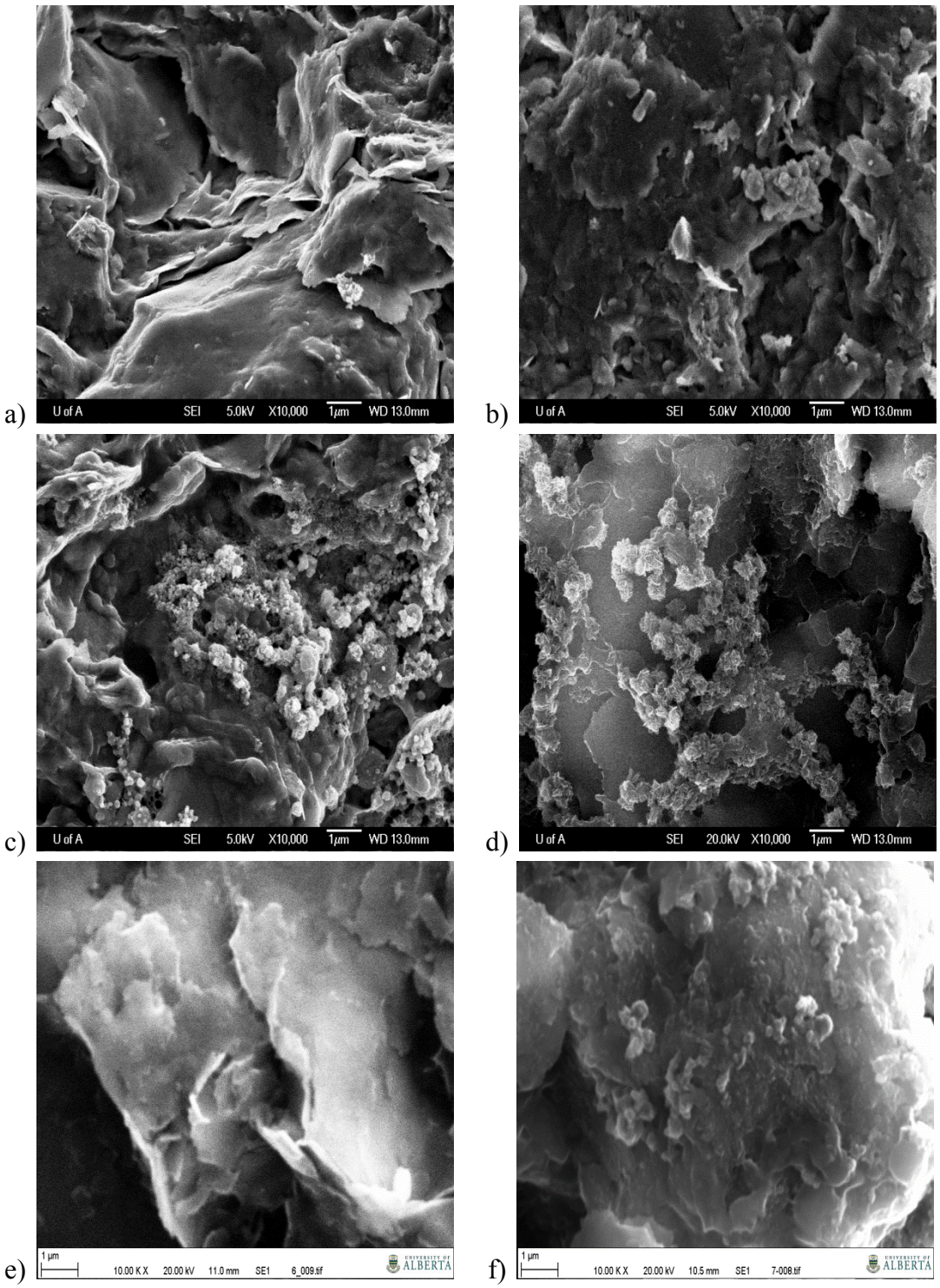

Figure 6-9 SEM images at 10,000X magnification. a) Intact; b) 48 hours; c) 216 hours; d) 384 hours; e) 552 hours and f) 1008 hours

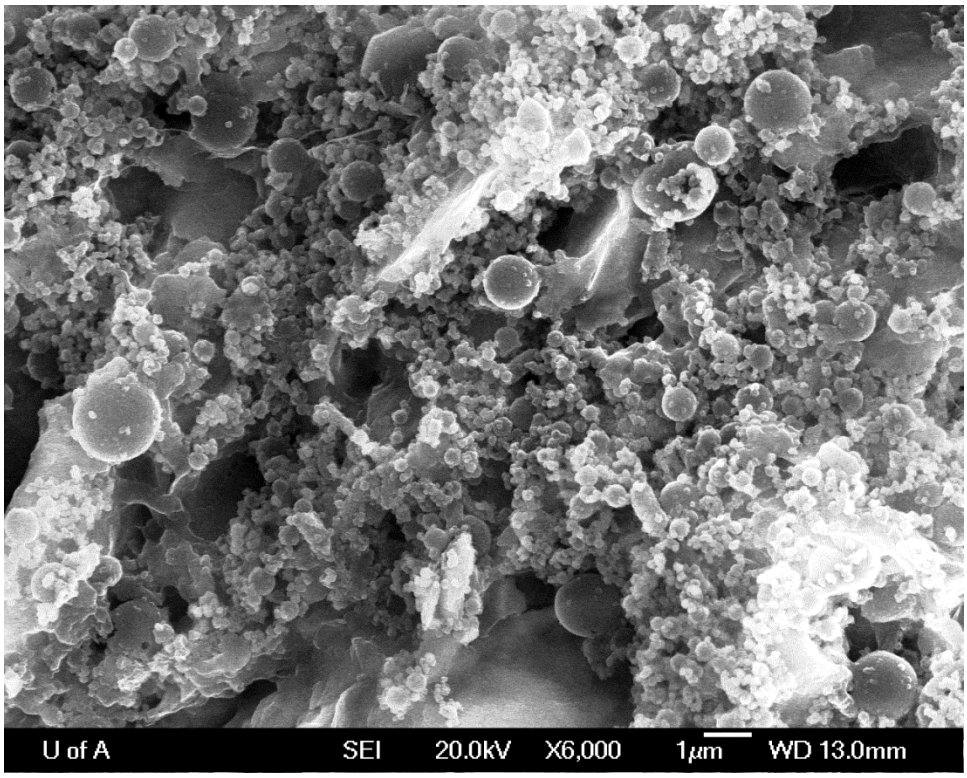

Figure 6-10 Cluster formed at sample surface (exposure time at 216 hours)

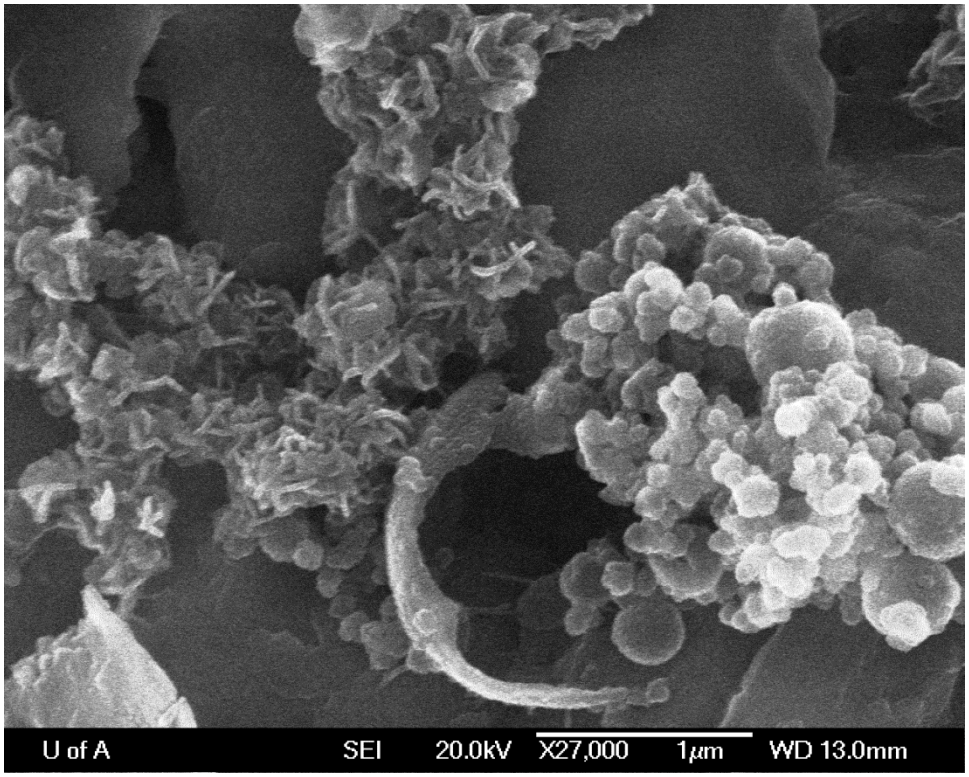

Figure 6-11 Cluster formed at sample surface (exposure time at 384 hours)

SEM results illustrate significant changes on Lea Park Shale surface due to CO_2 exposure:

- Intact Lea Park shale is highly argillaceous; also, small pores are observable.
- No obvious variations are noticed within the first 48 hours.
- Clusters began to form after 216 hours and at 384 hours; almost the entire shale surface was coated with cluster.
- With more exposure time, this cluster – coat disappeared and a newly clay-like material occupied the shale surface.

Images at higher magnifications show two types of cluster based on geometry, one is sphere-like and the other is chain-like.

6.1.3 Energy-dispersive X-ray Spectroscopy (EDS)

EDS was conducted during SEM imaging to generate addition data for chemical composition. Carbon concentration is not detectable through EDS so it is meaningless to compare these concentration values; ratios between different elements would best representative because of its independent of analysis method.

As discussed above, the growth and subsequent disappearance of various types of clusters were observed during the test using SEM. In order to understand the chemical composition of these clusters, EDS was introduced during SEM imaging. Firstly, the intact shale sample was scanned 5 times to obtain a general estimation of surface chemistry (Table 4-2). Following this general scan, 3 focussed scans were conducted on sphere-shaped cluster and chain-shaped cluster to estimate their chemical composition. As well, 3 additional scans were carried out on

Samples No.4 and No.5 to investigate the surface chemical composition after the cluster coating had disappeared. Average chemistry data on different materials was compared to the average values calculated from intact rock sample (Table 6-9).

Table 6-9 EDS scanning results

	Intact	Sphere	Chain	No.4	No.5
Na	0.47	0.89	0.22	0.62	0.67
Mg	0.78	0.77	0.65	1.22	0.88
Al	11.68	12.90	14.42	11.94	9.43
Si	31.49	30.36	25.47	25.43	23.00
K	3.21	2.71	4.67	3.62	2.76
Ca	0.26	0.44	0.40	0.18	0.00
Fe	3.44	3.31	8.23	3.35	3.43
O	48.68	48.59	45.90	52.02	48.78
S	0.00	0.02	0.05	0.00	0.12
Al/Si	0.37	0.42	0.57	0.47	0.41

The following observations were made based on the results from the EDS scanning:

- While not detected in XPS scanning, small amounts of magnesium and tiny amounts of sulfur were found with EDS.
- The chain-shaped cluster had an abnormal high concentration of iron, more than 2.5 times than other materials.
- The chain-shaped cluster had the largest ratio between aluminum and silicon weight concentration.
- The sphere-shaped cluster didn't have much difference in surface chemistry compared with the intact shale sample while the chain-shaped cluster had much larger chemical alterations.

- As exposure time increased, the cluster coating started to disappear and the surface chemistry is returned to initial intact condition.

- From SEM imaging (Figures 6-9 and 6-10) and EDS results (Table 6-9), for the first 48 hours, no significant reaction was detected. After 48hours, a sphere-shaped cluster-coating structure was discovered on the sample surface (216hours) and it gradually evolved into a chain-shaped cluster-coating structure (384 hours). These structures then disappeared upon continued exposure to CO_2–brine solution. Based on EDS scanning results, the sphere-shaped cluster-coating structure had almost the same signature as the intact shale material, but the later-formed chain-shaped cluster had higher Al/Si ratio (Table 6-9). So it is expected that the Al/Si will gradually increase from 0-384 hours, but the results from XPS are exactly the reverse (Table 6-8). No proper explanation was found for this discrepancy during the current research but it will be important for future research to confirm that repeatability of this process and its impact on the long term integrity of the caprock.

6.2 Permeability Measurement

Measurements of permeability were conducted on two shale specimens using the pulse decay method prior to capillary breakthrough test. Pressure-time data within first hour was recorded.

6.2.1 Permeability Measurement for LP1

Permeability measurement was carried out on specimen LP1 at in-situ stress conditions. Figure 6-13 shows the results of permeability measurement with 0.5 MPa increment at upstream.

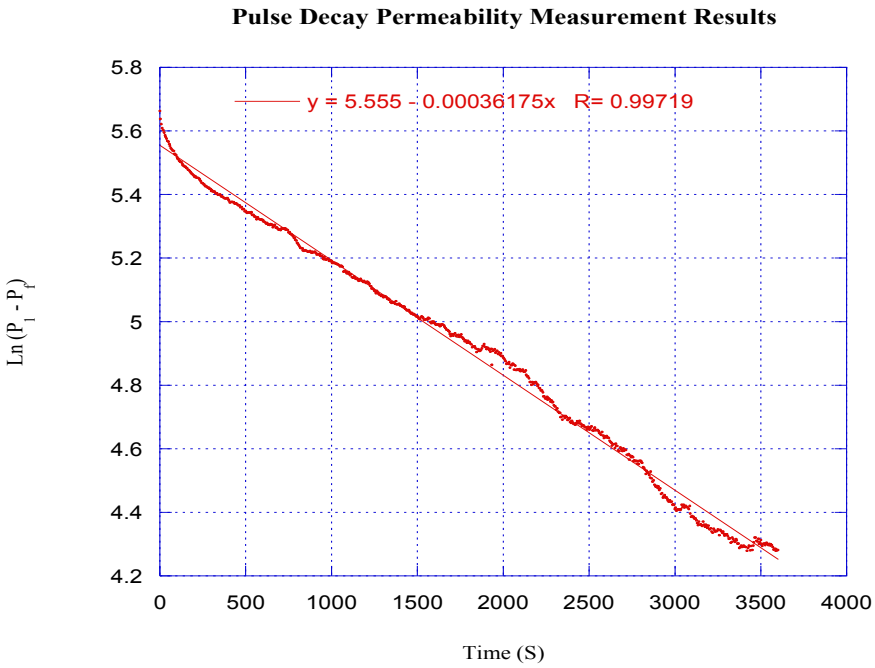

Figure 6-12 Permeability measurement for LP1at 28.5MPa Confining pressure and 50°C

The calculated slope in Figure 6-13 is -0.00036. Using this value along with the following parameters, equation [2] is used to compute permeability.

$\alpha = -3.62*10^{-4}\ s^{-1}$

$A = 2.84*10^{-3}\ m^2$

$\mu = 5.53*10^{-5}$ dyne* sec*cm^{-2} [1]

$\beta = 3.52*10^{-11}\ cm^2*dyne^{-1}$

$L = 2.67*10^{-2}\ m$

$V_1 = 6.02*10^{-5}\ m^3$

$V_2 = 7.56*10^{-5}\ m^3$

The measured permeability is: $k = 2.2*10^{-22}\ m^2 = 0.22$ nD

6.2.2 Permeability Measurement for LP2

As noted previously, several fissures were observed in the LP2 shale sample. To assess how the permeability would change with effective confining pressure, the

confining pressure was increased from 28.5 to 33 MPa in 1.5 MPa intervals and at each step, a permeability measurement was conducted. The backpressure (pore pressure) was held constant at 15 MPa and the permeability measurement was conducted at each stage 24 hours after the confining pressure was increased (to let the sample to fully consolidate).

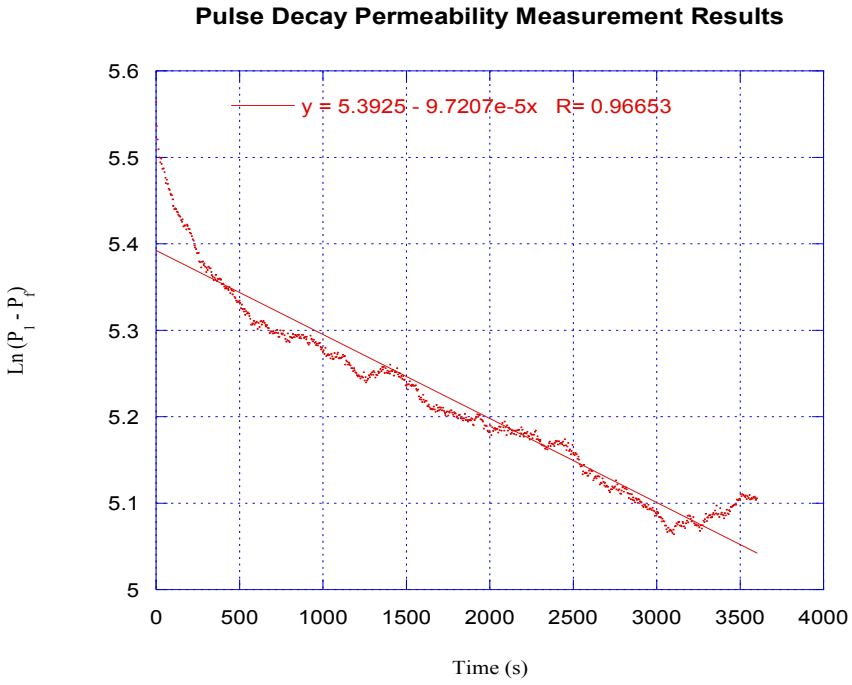

Figure 6-13 Permeability measurement for LP2 at 28.5MPa confining pressure and 50°C

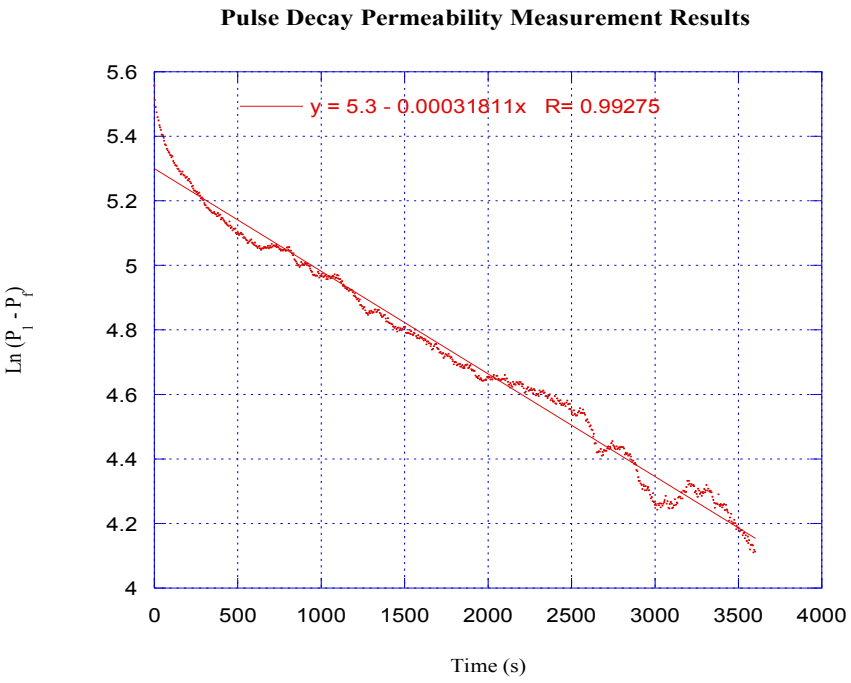

Figure 6-14 Permeability measurement for LP2 at 30MPa confining pressure and 50°C

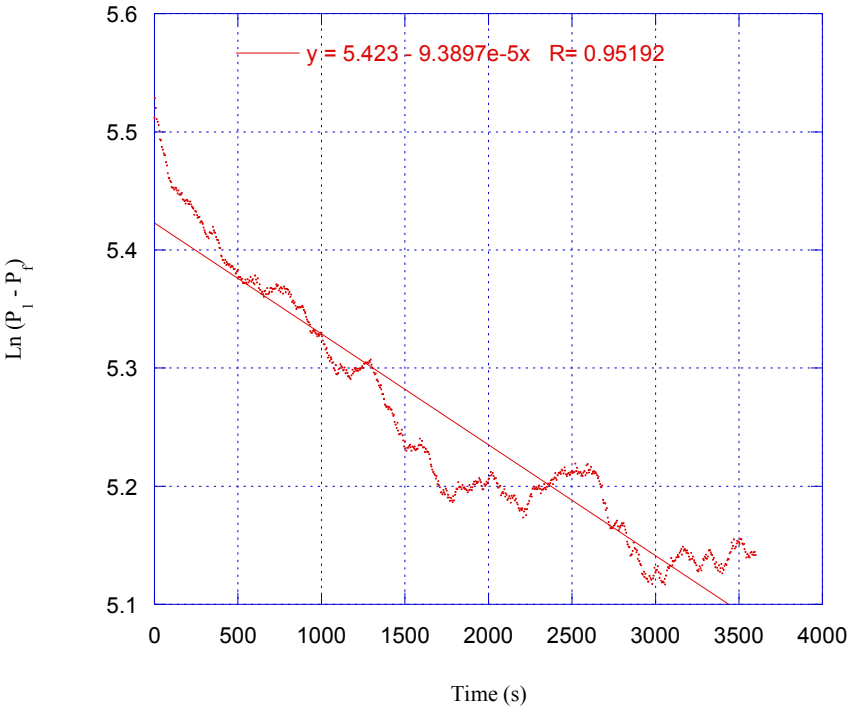

Figure 6-15 Permeability measurement for LP2 at 31.5 MPa confining pressure and 50°C

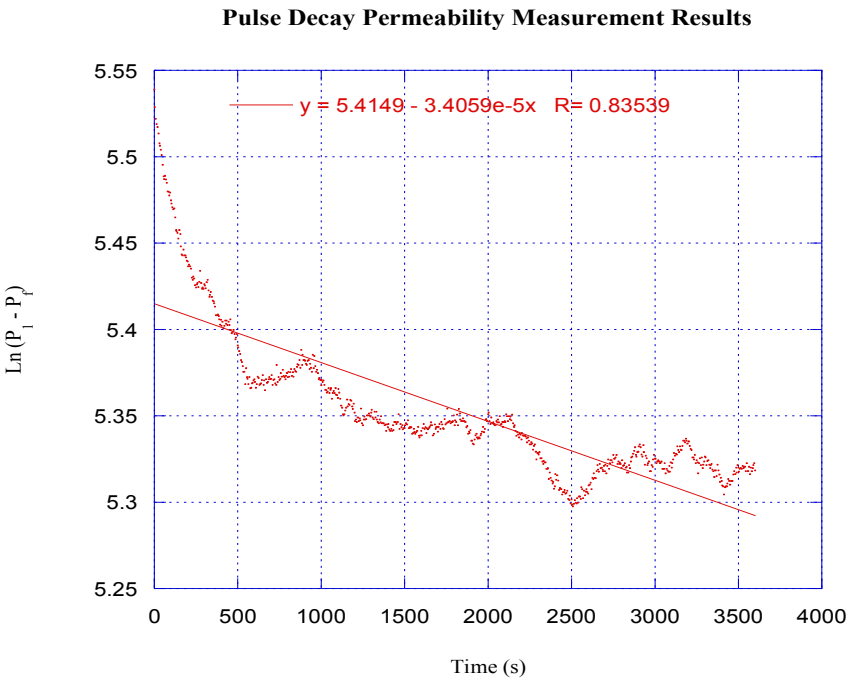

Figure 6-16 Permeability measurement for LP2 at 33MPa confining pressure and 50°C

Permeability for LP2 was calculated with the same parameters used for LP1, except for sample dimension. Results of the permeability measurements for LP2 at different confining pressure are presented in Table 6-10. It was found that permeability did not change significantly with the build-up of confining pressure which likely indicates the fissures had already closed upon the application of the in situ stress conditions.

Table 6-10 Permeability for sample LP2 at different confining pressures

Confining Pressure (MPa)	Slope ($-10^{-5}*s^{-1}$)	Permeability ($10^{-22}*m^2$)
28.5	9.72	4.38
30.0	31.8	14.33
31.5	9.39	4.23
33.0	3.41	1.54

6.2.3 Systematic Error

As discussed previously, one of the weak assumptions in Brace's method is that the sample porosity and compressive storage are very small and can be neglected. However, for the class of shales tested in this research, this assumption is not valid since the porosity and compressive storage are very large compared to granites. Based on Trimmer, in order to have a systematic error of l0% or less, the ratio between effective sample pore volume and reservoir volume should be kept below 0.25.

Previous laboratory investigations have been conducted on the same rock core at GeoREF Lab in University of Alberta and the results showed that the porosity of Lea Park shale lies between 9.1% and 13.0% with an average value of 12.8%. Meanwhile, the volume of upstream reservoir is 60.2mL. Sample volume was calculated using sample dimensions. The calculated ratios between sample pore volume and upstream volume for both samples were 0.16 and 0.19. Since effective sample volume is smaller than total sample pore volume, the above ratio would be even smaller. Based on the above calculation, the ratios between effective sample pore volume and reservoir volume are smaller than 0.25 for both samples, it is considered that the test results have a systematic error of less than 10% and the measured permeability is reliable.

6.3 Capillary Breakthrough Test

Following the permeability test, the system is left to stabilize for a period of 24 hours before conducting capillary entry pressure measurements using the small increment method.

6.3.1 Capillary Entry Pressure Measurement on LP1

Based on the previous test experience and the fact that this shale material may contain some fissures, it was expected that the capillary entry pressure would be relatively small. Consequently, what were thought to be very small pressure increments of 0.5 MPa were adopted initially. However, this 0.5 MPa "small" increment is actually too large for this shale material and breakthrough happened very quickly after the second increment, so capillary entry pressure could not be accurately measured for sample LP1. Based on the data, the capillary entry pressure for sample LP1 is between 500 and 1,000 kPa.

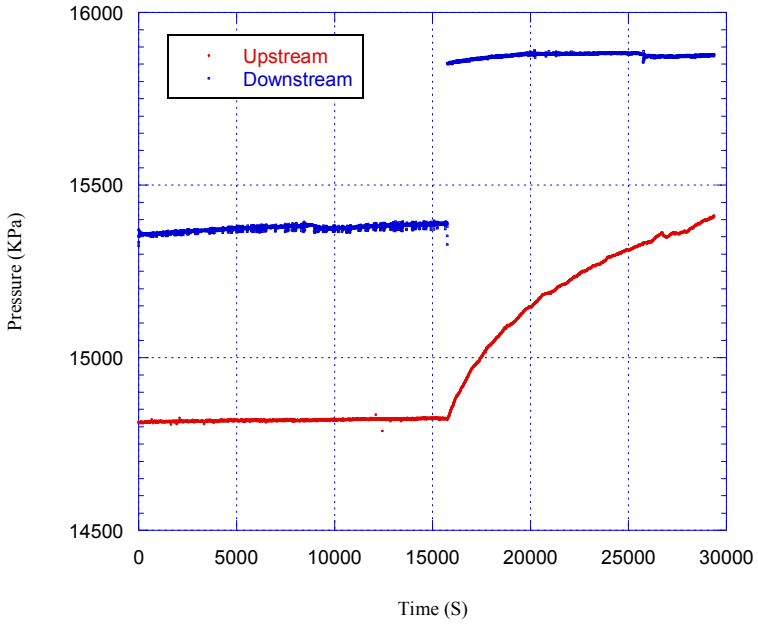

Figure 6-17 Capillary entry pressure measurement for LP1

6.3.2 Capillary Entry Pressure Measurement on LP2

Based on experience gained from the LP1 test, the pressure increment was reduced to 100 kPa for sample LP2. Figures 6-18 and 6-19 illustrate the results from the tests. Cumulative flow rate (the average flow rate since the start of the

test) was recorded with time and the results indicate that the measured capillary entry pressure of sample LP2 is 700kPa.

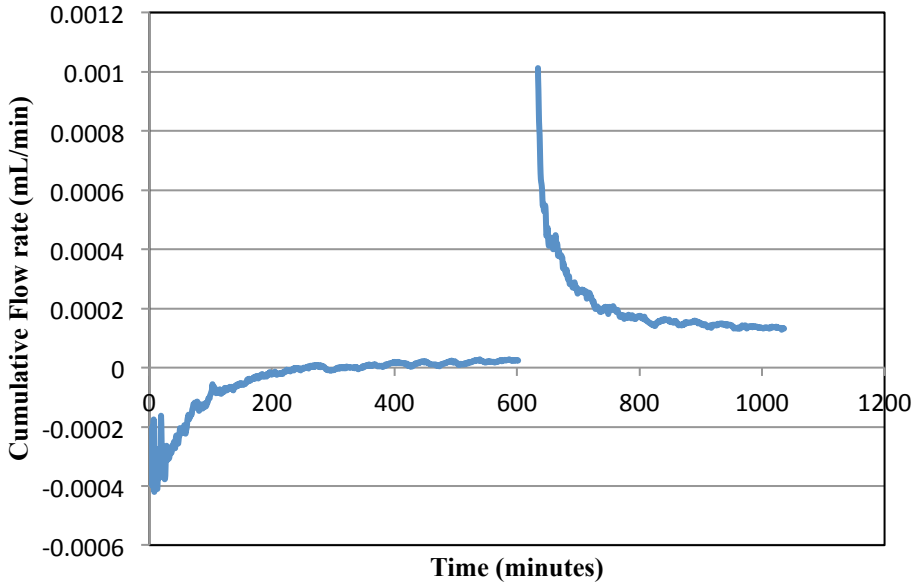

Figure 6-18 Cumulative flow rate of upstream brine pump for LP2

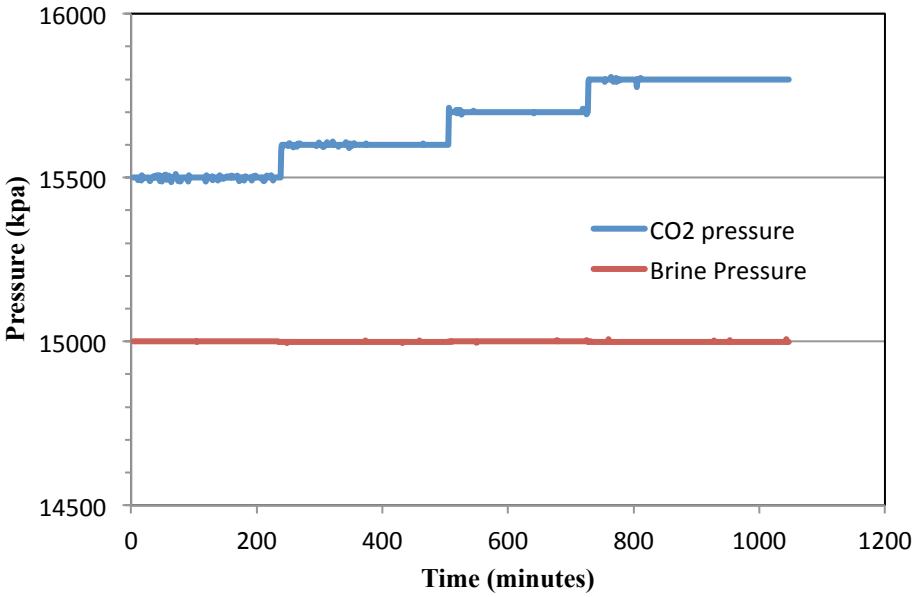

Figure 6-19 Pressure reading for both brine and CO_2 pumps for LP2

6.4 Chapter Summary

Dissolution of illite, growth and then disappearance of different types of cluster-coating structures were observed due to Lea Park shale/brine/CO_2 interactions. Also, it is found out that Lea Park shale is a material with low capillary entry pressure (700kPa) and ultra-low permeability (less than 1nD).

6.5 Reference

1. Kestin, J., H. Khalifa and R. Correia, 1981. Tables of the dynamic and kinematic viscosity of aqueous NaCl solutions in the temperature range 20-150°C and the pressure range 0.1-35 MPa. Journal of Physical and Chemical Reference Data, Vol. 10, pp. 71-86.

2. Onori, G., 1988. Ionic hydration in sodium chloride solutions. J. Chem. Phys, Vol. 89, pp. 510-516.

7 Conclusions and Recommendations

The following summarizes the major conclusions reached from the entire research programme. This is followed by recommendations for future research in this area.

7.1 Conclusions

Major conclusions from this experimental investigation are as follows:

- Lea Park shale contains reactive minerals so shale/brine/CO_2 interaction plays role in carbon geosequestration and should be considered in storage assessments.
- Injection of CO_2 causes dissolution of illite within the Lea Park shale and dissolution of silicon.
- Rock/Brine/CO_2 causes growth of cluster-coating structures on the surfaces of the Lea Park shale sample and will eventually disappear.
- Two different types of cluster-coating structures were found due to CO_2 exposure based on geometry. After CO_2 injection, a sphere-shaped cluster-coating structure will first appear on the surface of Lea Park shale and this sphere-shaped cluster-coating structure will gradually transfer into another chain-shaped structure; finally, all the cluster-coating structures will disappear and the surface chemistry of Lea Park shale rebound to initial state.
- The measured permeability for Lea Park shale at 28.5MPa confining and 50°C ranges from 0.22 to 0.44nD.
- The CO_2 breakthrough pressure for Lea Park shale determined in this research program is 700kPa.
- Lea Park shale is a material with very low capillary entry pressure (less than 1MPa) and ultra-low permeability (less than 1nD). So even though

injected CO_2 could easily penetrate into caprock formation but will be trapped in the formation for a very long period due to its ultra-low permeability.

7.2 Recommendations

While a number of tests were conducted in this research, additional work is definitely required to continue building our knowledge of how these shale caprock systems evolve upon exposure to CO_2/brine mixtures.

- The shale specimen/CO_2/brine reaction tests were only conducted at 2 MPa due to the low strength of plastic holder system. It is important for future tests to be conducted at higher pressures to better reflect in situ conditions. This will require a redesign of the shale specimen bonding system.
- After CO_2 injection, cluster-coating structures were detected on the shale surface and all the cluster-coating structures disappeared after relatively long term period. The impact of this process on the strength of caprock needs to be investigated to ensure caprock integrity.
- The exposure time of Lea Park shale in this research program is relatively short compared with field practice, longer exposure time could be considered in future research.
- Flow numerical modeling should be introduced based on data from this research program to better understand the long-term sealing potential of the Lea Park shale as a caprock for CO_2 geological storage sites within the Pembina Cardium field.
- Geochemical modeling could be considered with the data from this research program to better understand the geochemistry during CO_2 injection.

- The capillary breakthrough test adopted in this research project only generates results for absolute threshold capillary pressure. Further investigations on capillary pressure versus CO_2 saturation are recommended to approach in situ conditions.

Appendix A: Cell Reaction Test Procedures

The standard test procedure for the cell reaction tests are:

1. Spread vacuum grease on the inside of both cells for mold preparation. Be careful with the distribution and thickness of grease, it should be as even as possible and neither too thick nor too thin.
2. Tighten all fittings, apply low pressure, use liquid leak detector to check system leakage for both cells.
3. Fill both cells with some brine solution and place pre-manufactured plastic holding samples in saturation cell.
4. Apply 2MPa to saturate the sample, recording pressure and temperature periodically.
5. Conduct XPS scanning on saturated samples for intact rock chemical composition information.
6. Re-saturate samples after XPS scanning.
7. Turn on heating device and set temperature at 50°C on reaction cell, wait until temperature reading is stable.
8. Transfer brine saturated samples into reaction cell (for blank test samples, remain them in saturation cell), close the seal, and apply continuous CO_2 flow for 2 minutes to drive all the air out of cell, then close inlet valve.
9. Check pressure and temperature periodically.
10. Remove sample from cell at pre-designed time, carried out XPS scanning, SEM imaging and EDS analysis.

Appendix B: Calibration of Pressure Transducers

In addition to pump pressure readings, four pressure transducers were attached in the system: one each for measuring confining pressure, upstream pressure and downstream pressure, and the fourth transducer measuring the differential pressure between the upstream and downstream lines. Honeywell FPG pressure transducer with a maximum pressure reading of 34.5 MPa (5,000 psi) was used to measure the confining, upstream and downstream pressure while differential pressure was recorded by VALIDYNE DP15-TL pressure transducer. The Honeywell pressure transducers were calibrated with using a hydraulic deadweight tester over the pressure range 0.7 to 27.6 MPa (100 to 4000 psi) while the Validyne transducer was calibrated from 0.7 to 22.8 MPa (100 to 3300 psi). Figures 5-14 to 5-17 illustrate the results of calibration. This calibration information was then entered into the data acquisition system.

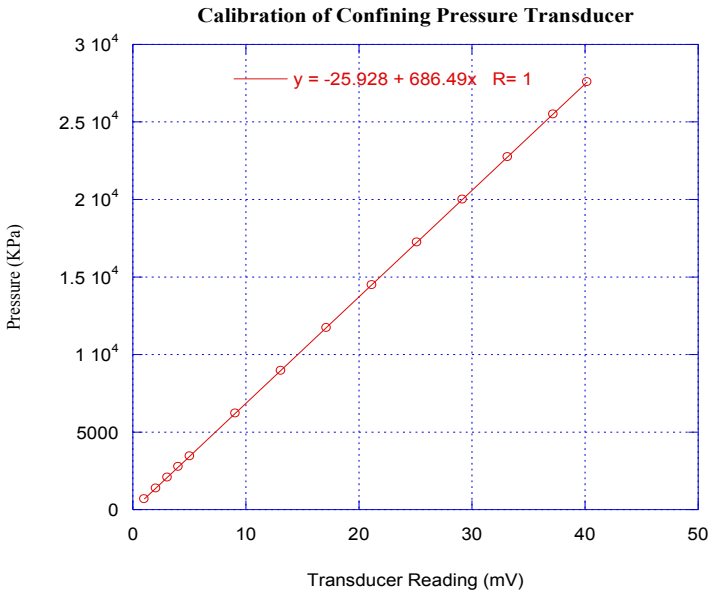

Figure B-1 Calibration of confining pressure transducer

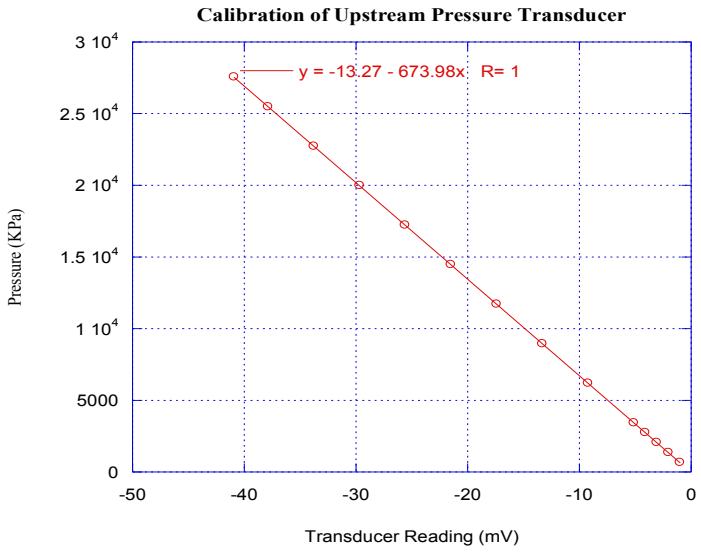

Figure B-2 Calibration of upstream pressure transducer

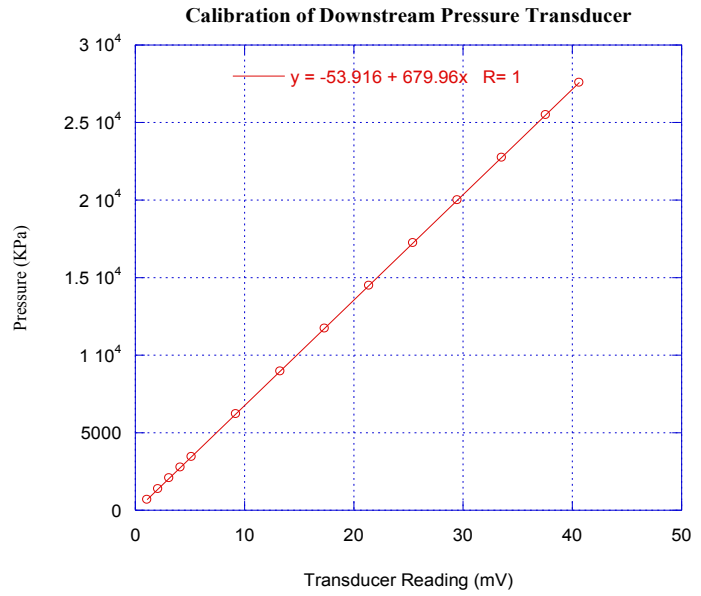

Figure B-3 Calibration of downstream pressure transducer

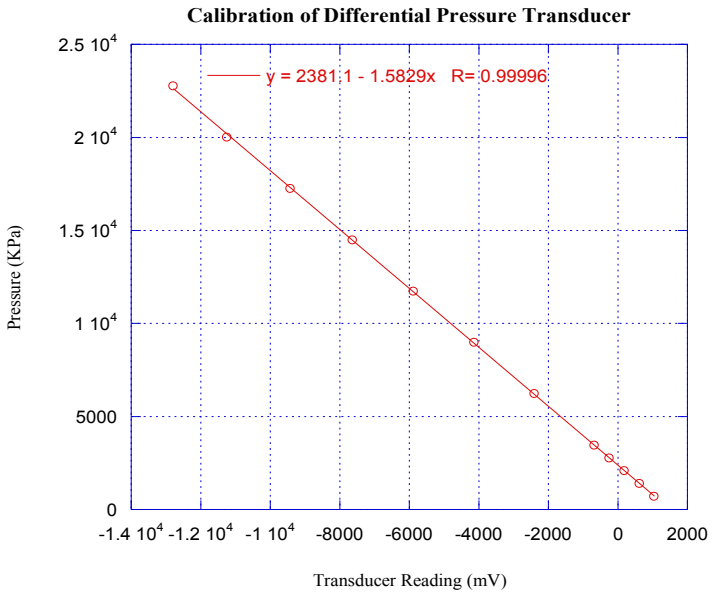

Figure B-4 Calibration of differential pressure transducer

Appendix C: Procedures for Permeability Measurement

Permeability measurement using the pulse decay method was conducted with using the following procedures:

- After the consolidation stage was finished, valve “a” and “bypass” are closed.
- Increase Pump A pressure from 15.0 to 15.5 MPa and after the pump pressure reading is stable, quickly open and then close valve “a” to introduce the pulse.
- Record pressure data in both upstream and downstream reservoirs.

Appendix D: Procedures for Capillary Pressure Measurement

After completion of the permeability measurement, a capillary breakthrough test was carried out on shale specimen using the large increment method through the following procedures:

- Gradually reduce the confining pressure and back pressure to 14 MPa and 0.5 MPa respectively.
- Close "bypass" valve, open valve "d", apply a continuous N_2 gas flow in downstream reservoir at 0.5 MPa for 15 minutes to blowout all the fluid in downstream reservoir.
- Replace N_2 gas flow with CO_2 air flow, similarly, let the CO_2 flow for 5 minutes, then close valve "d".
- Gradually increase confining pressure, upstream reservoir brine pressure and downstream reservoir CO_2 pressure to 28.5, 15 and 15 MPa respectively. Let the system stabilize for 24 hours.
- Increase Pump C pressure by 0.5 MPa and keep it constant, record pressure, flow rate and volume of pump A and B.